1 2005

AFRL-SR-AR-TR-05-

0536

REPORT DOCUMENTATION PAGE

The public reporting burden for this collection of information is estimated to average 1 hour per response, including the time for reviewing instructions, searching existing data sources, gathering and maintaining the data needed, and completing and reviewing the collection of information. Send comments regarding this burden estimate or any other aspect of this collection of information, including suggestions for reducing the burden, to Department of Defense, Washington Headquarters Services, Directorate for Information Operations and Reports (0704-0188), 1215 Jefferson Davis Highway, Suite 1204, Arlington, VA 22202-4302. Respondents should be aware that notwithstanding any other provision of law, no person shall be subject to any penalty for failing to comply with a collection of information if it does not display a currently valid OMB control number.
PLEASE DO NOT RETURN YOUR FORM TO THE ABOVE ADDRESS.

1. REPORT DATE (DD-MM-YYYY)	2. REPORT TYPE	3. DATES COVERED (From - To)
01/26/2005	Final Report	12/15/00 - 03/15/04

4. TITLE AND SUBTITLE

Carbothermal Reduction Synthesis and Structural Evolution of Nanocrystalline Ultra High Temperature Carbides

5a. CONTRACT NUMBER

5b. GRANT NUMBER

F49620-01-1-0112

5c. PROGRAM ELEMENT NUMBER

6. AUTHOR(S)

Michael D. Sacks

5d. PROJECT NUMBER

E-18-651

5e. TASK NUMBER

5f. WORK UNIT NUMBER

7. PERFORMING ORGANIZATION NAME(S) AND ADDRESS(ES)

Georgia Tech Research Corporation
505 Tenth Street
Atlanta, GA 30332-0420

8. PERFORMING ORGANIZATION REPORT NUMBER

9. SPONSORING/MONITORING AGENCY NAME(S) AND ADDRESS(ES)

Dr. Joan Fuller
Air Force Office of Scientific Research
4015 Wilson Blvd., Room 713
Arlington, VA 22203-1977

10. SPONSOR/MONITOR'S ACRONYM(S)

AFOSR

11. SPONSOR/MONITOR'S REPORT NUMBER(S)

12. DISTRIBUTION/AVAILABILITY STATEMENT

No distribution restrictions

13. SUPPLEMENTARY NOTES

14. ABSTRACT

Zirconium carbide (ZrC) and hafnium carbide (HfC) powders were produced by the carbothermal reduction reaction of carbon and the corresponding metal oxide (ZrO2 and HfO2, respectively). Solution-based processing was used to achieve a fine-scale (i.e., nanometer-level) mixing of the reactants. The reactions were substantially completed at relatively low temperatures (<1500C) and the resulting products had small average crystallite sizes (~50-130 nm). Dry-pressed compacts prepared using ZrC-based powders with ~100 nm crystallite size could be pressurelessly sintered to ~99% relative density and zero open porosity at 1950C. Silicon carbide (SiC) powders with crystallite size <25 nm were prepared at low temperature (~1300C) by carbothermal reduction reactions in silica/carbon mixtures. Solution-based processing was again used to achieve fine-scale mixing of the reactants. Mechanistic studies indicated that the SiC formed in accordance with the "shrinking core" reaction model in which the rate was controlled by the reaction of silicon monoxide vapor at carbon surfaces.

15. SUBJECT TERMS

16. SECURITY CLASSIFICATION OF:			17. LIMITATION OF ABSTRACT	18. NUMBER OF PAGES	19a. NAME OF RESPONSIBLE PERSON
a. REPORT	b. ABSTRACT	c. THIS PAGE			Michael D. Sacks
U.	U.	U.	UU	62	19b. TELEPHONE NUMBER (Include area code) 404-385-0624

Approved for Public Release
Distribution Unlimited

CARBOTHERMAL REDUCTION SYNTHESIS AND STRUCTURAL EVOLUTION OF NANOCRYSTALLINE ULTRAHIGH TEMPERATURE METAL CARBIDES

Final Report (12/15/00 - 3/15/04)

AFOSR Grant No. F49620-01-1-0112

Submitted to:

Air Force Office of Scientific Research
Room 732
801 N. Randolph Street
Arlington, VA 22203-1977

Submitted by:

M.D. Sacks
School of Materials Science and Engineering
Georgia Institute of Technology
Atlanta, GA 30332-0245

20050218 061

December 2004

TABLE OF CONTENTS

ABSTRACT

Zirconium carbide (ZrC) and hafnium carbide (HfC) powders were produced by the carbothermal reduction reaction of carbon and the corresponding metal oxide (ZrO_2 and HfO_2, respectively). Solution-based processing was used to achieve a fine-scale (i.e., nanometer-level) mixing of the reactants. The reactions were substantially completed at relatively low temperatures ($<1500°C$) and the resulting products had small average crystallite sizes ($\sim$50-130 nm). Dry-pressed compacts prepared using ZrC-based powders with $\sim$100 nm crystallite size could be pressurelessly sintered to $\sim$99% relative density and zero open porosity at 1950°C.

Silicon carbide (SiC) powders with crystallite size <25 nm were prepared at low temperature ($\leq$1300°C) by carbothermal reduction reactions in silica/carbon mixtures. Solution-based processing was again used to achieve fine-scale mixing of the reactants. Mechanistic studies indicated that the SiC formed in accordance with the "shrinking core" reaction model in which the rate was controlled by the reaction of silicon monoxide vapor at carbon surfaces.

LIST OF FIGURES

LIST OF TABLES

1.0 EXECUTIVE SUMMARY

This project focused primarily on the synthesis and structural evolution of nanocrystalline zirconium carbide (ZrC), hafnium carbide (HfC), and silicon carbide (SiC) powders. These refractory carbide materials are of interest for ultrahigh temperature applications requiring improved thermomechanical and thermochemical stability, such as for components used in heat engines and in thermal protection systems for advanced aerospace applications.

The powders synthesized in this study were produced by carbothermal reduction (CTR) using fine-scale carbon/metal oxide mixtures as starting materials. The reactant mixtures were prepared by pyrolytic decomposition of solution-derived precursors. The specific elements of this project included the following: (i) development of solution-based synthesis methods for preparation of the reactant mixtures, (ii) investigation of the effects of selected solution-processing variables and subsequent heat treatment conditions on the synthesized carbide powder characteristics, (iii) characterization of the reaction products using techniques such as X-ray diffraction, thermal analysis, gas adsorption, electron microscopy, etc., and (iv) preliminary investigation of the sinterability of synthesized carbide powders.

The solution-based synthesis methods involved steps the following processing steps: synthesis and/or modification of soluble metal-organic compounds, mixing of the soluble precursors, carrying out controlled hydrolysis/condensation reactions, and removing solvent from processed solutions. Solution-processing variables investigated included the type and concentrations of starting materials, conditions used to modify the metal-organic compounds (e.g., concentration of modifying compound, processing temperature, etc.), and concentrations of water and acid used during hydrolysis/condensation reactions. Processing variables investigated during subsequent heat treatments steps (i.e., pyrolytic decomposition of dried precursors and CTR of reactant mixtures) included temperature, time, and gas flow conditions. The resulting carbide powders were characterized to determine characteristics such as particle/aggregate size, specific surface area, phases present, chemical composition, lattice parameter, etc.

Detailed studies of phase development during the CTR formation of ZrC and HfC were carried out using pyrolyzed powder with carbon/metal oxide ratios ≈3.1. The pyrolyzed powders consisted of fine-scale mixtures of the tetragonal phase of the metal oxide (zirconium oxide or hafnium oxide) and amorphous carbon. The initial formation of the metal carbide (ZrC or HfC) was clearly evident after heat treatment at 1200°C and the reaction was substantially completed after heat treatments in the range of ~1400-1500°C. HfC and ZrC powders produced at 1475°C had crystallite sizes were ~50 nm and ~100-130 nm, respectively. ZrC powders with ~100 nm crystallite sizes were dry-pressed to form powder compacts with ~44% relative density. Compacts which were sintered (without any external applied pressure) at 1900°C and 1950°C had relative densities of ~98% and ~99%, respectively, and zero open porosity.

In the SiC study, the CTR mechanism was investigated by analyzing condensates of volatile species generated during the reaction, determining isothermal reaction kinetics in mixtures with initial C/Si molar ratios of 2.4 and 4.6, and characterizing the product structural evolution throughout the reaction. The results indicated that the CTR reaction was a multi-step process that involved silicon monoxide (SiO) as a reaction intermediate. The reaction kinetics showed an excellent fit to the "shrinking-core" model in which an interfacial reaction was the rate-controlling step. The available evidence indicated that the reaction between SiO vapor and carbon (at carbon surfaces) was the rate-controlling step. Using a reactant mixture with C/Si molar ratio of 2.4, it was possible to prepare a product which was mostly converted to β-SiC with average crystallite size <25 nm after CTR heat treatment at 1300°C for 16 h.

This report includes the following sections: introductory background information on processing of ZrC, HfC, and SiC (section 2.0); research approach and experimental methods utilized in this study (section 3.0); results and discussion (section 4.0); conclusions (section 5.0); references (section 6.0). In addition, a complete list of the publications resulting from this project is provided in the Appendix (section 7.0). More detailed information concerning the research approach, experimental methods used,

data collected, and analysis and discussion of results for this project are given in the following graduate student theses which were completed through the support provided by this project: (1) Anubhav Jain, "Synthesis and Processing of Nanocrystalline Zirconium Carbide Formed by Carbothermal Reduction," M.S. Thesis, Georgia Institute of Technology, August 2004. (2) Zhe Cheng, "Reaction Kinetics and Structural Evolution for the Formation of Nanocrystalline SiC via Carbothermal Reduction," M.S. Thesis, Georgia Institute of Technology, December 2004.

2.0 INTRODUCTION

2.1 Zirconium Carbide (ZrC) and Hafnium Carbide (HfC)

Zirconium carbide (ZrC) and hafnium carbide (HfC) are of interest for ultrahigh temperature applications because of their high melting points (~3550°C and ~3900°C, respectively), solid-state phase stability, and good thermomechanical and thermochemical properties.[1-5] Other desirable properties of ZrC and HfC include high hardness and wear resistance, high emissivity, and high current capacity at elevated temperatures. Hence, these carbides are promising materials for cutting tools, thermophotovoltaic radiators, and field emitter tips and arrays.[1,2,6,7] In addition, ZrC is useful as a nuclear reactor core material because of its low neutron cross-section.[8]

ZrC and HfC are usually synthesized by reacting powder mixtures of carbon and the corresponding metal (Hf, Zr), metal hydride (ZrH_2, HfH_2), or metal oxide (ZrO_2, HfO_2).[1,2,5,6,9-13] In most cases, high temperatures are required for the carbide-forming reactions because the powders are mixed together on a relatively coarse scale (e.g., micrometer-scale). This also leads to metal carbide products with relatively large particle sizes. Hence, hot pressing is usually necessary to produce bulk objects with high relative densities.

Recent studies have shown that ZrC and HfC can be synthesized at lower temperatures by using precursors that have been prepared by solution-based processing methods.[14-18] Sham et al. synthesized ZrC powders using mixed solutions of zirconium n-propoxide (as a zirconia source) and either ethylene glycol or 1,4 benzenediol (as a carbon source).[14] Preiss et al. used chelated derivatives of zirconium n-propoxide and various soluble carbon-bearing compounds (including those used by Sham et al.) to form ZrC fibers, films, and powders.[15] Hasegawa et al. used mixtures of zirconium 2,4,-pentanedionate and phenolic resins to produce ZrC fibers with diameter ≥60 μm.[16] Hu et al. used the same mixtures to produce nanocrystalline ZrC powders and fibers with ~20 μm diameter.[17] Kurokawa et al. produced large-diameter (≥50 μm) ZrC and HfC fibers by using solutions containing cellulose acetate and metal

alkoxides (zirconium n-butoxide and hafnium isopropoxide) as the precursors for the carbon and metal oxides, respectively.[18] The aforementioned studies all showed (via X-ray diffraction analyses) that ZrC or HfC phases can be formed at relatively low temperatures compared to conventional methods. However, very little information on the densification behavior of these materials was presented and it was not reported if bulk samples could be fabricated by pressureless sintering.

In the present study, ZrC- and HfC-based precursors with a range of carbon/metal oxide ratios were prepared from chelated derivatives of metal alkoxides by varying the hydrolysis conditions and by adding soluble secondary "carbon sources" (i.e., glycerol and phenolic resin) during solution-based synthesis. The solution-derived precursors were given heat treatments (pyrolysis and carbothermal reduction) to produce nanocrystalline ZrC and HfC powders. Pressureless sintering of the ZrC powder was investigated.

2.2 Silicon Carbide (SiC)

The primary industrial method for manufacturing silicon carbide (SiC), the Acheson process, involves the carbothermal reduction reaction of silica and carbon using coarse mixtures prepared from relatively inexpensive raw materials (i.e., sand and coke). The process requires high temperature (>2200°C) for extensive reaction to occur and the resulting SiC must undergo various grinding and purification steps to produce powders that are suitable for technical ceramics.[19] Hence, many methods have been developed to prepare SiC by using starting materials that allow for a finer scale of mixing of the silica and carbon reactants in comparison to the conventional industrial process.[20-27] Solution-based processing routes are particularly useful in this regard and such methods have been used successfully to prepare fine-grained SiC powders at much lower processing temperatures.[24-27] However, there are relatively few studies with solution-processed materials that have been directed toward understanding the mechanisms of the carbothermal reduction reaction.

In the present study, nanocrystalline SiC was prepared using solution-based processing in which

tetraethoxysilane (TEOS) was the silica-bearing precursor and phenol-formaldehyde resin was the carbon-bearing precursor. The carbothermal reduction reaction kinetics and structural evolution of the reaction product were investigated using two different carbon/silica ratios.

3.0 EXPERIMENTAL PROCEDURES

3.1 Zirconium Carbide (ZrC) and Hafnium Carbide (HfC)

3.1.1 General Methodology

The processing steps used to produce ZrC and HfC are initially described below in broader terms in order to provide the rationale for the synthesis methodology. This is followed by the specific experimental details used in the synthesis and characterization of each individual metal carbide.

The synthesis approach is illustrated via the flow chart in Fig. 1. A metal alkoxide, either self-synthesized or obtained from a commerical vendor, was used as an alcohol-soluble precursor for the formation of the metal oxide reactant needed for the carbothermal reduction reaction. The metal alkoxide is refluxed with 2,4 pentanedione (also known as acetylacetone and often referred to as "acacH") in order to partially or fully convert the metal alkoxy groups to a chelated metal diketonate structure (i.e., a metal pentanedionate, or "metal acac," in this case). (The extent of replacement depends on factors such as the reflux time/temperature schedule, "acacH"/metal alkoxide ratio, and solvent concentration.) The primary reason for carrying out the replacement reaction is to produce a soluble metal-organic precursor that allows for greater control over the hydrolysis and condensation reactions that are carried out in a subsequent processing step. In general, metal alkoxides undergo more rapid hydrolysis/condensation reactions than the corresponding metal diketonates and this may result in uncontrolled precipitation of relatively large precursor particles. The replacement reaction also allows for more control over the carbon/metal oxide ratio in the pyrolyzed powders that are subsequently produced (and used for the carbothermal reduction reactions). For example, pyrolyzed materials with higher carbon contents can be obtained by using precursors with a higher degree of replacement of the alkoxide groups. The flow chart in Fig. 1 also shows that another method for increasing the carbon/metal oxide ratio in the pyrolyzed product is to combine the metal-organic precursor with a soluble carbon-bearing source in a mutually compatible solvent. This can be done prior to or after the "acacH" refluxing step.

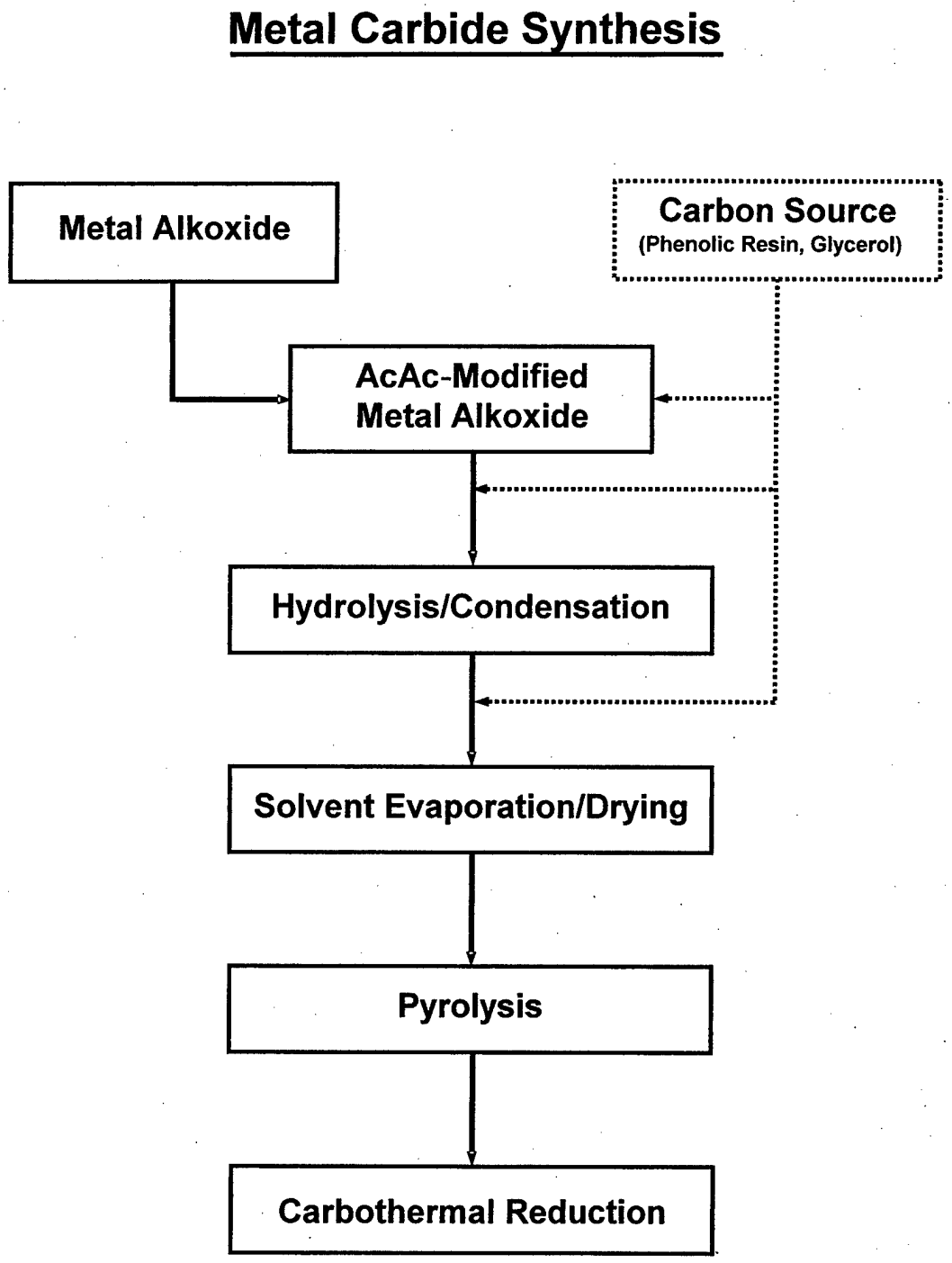

Fig. 1. Flow chart for synthesis of metal carbide from solution-based precursors

The next solution processing step is to hydrolyze the metal-organic precursor through the addition of water. Hydrolysis is required to initiate condensation reactions which, in turn, lead to the build-up of sol species with three-dimensional structure. (The latter development is important in order to obtain a reasonable ceramic yield upon subsequent pyrolytic decomposition.) The extent of the hydrolysis/ condensation reactions depends on the water concentration and solution pH. The latter variables can be used to alter the size and chemical composition (i.e., metal/oxygen/carbon content) of the sol species (and the powder product that is subsequently obtained).

After the hydrolysis/condensation step, the solvent is evaporated and a dried powder product is obtained. This is followed by sequential heat treatments to (i) pyrolytically decompose the dried product and thereby form a nano-scale carbon/metal oxide mixture and (ii) form the metal carbide by carbothermal reduction reactions.

3.1.2 Zirconium Carbide (ZrC)

The starting Zr-containing material was a zirconium n-propoxide/n-propanol solution (i.e., 70 wt% $Zr(OC_3H_7)_4$ in n-propanol, Alfa Aesar, Ward Hill, MA). The zirconium n-propoxide was mixed with "acacH" (i.e., 2,4-pentanedione, Alfa Aesar, Ward Hill, MA) using molar ratios in the range of 0.25-0.33. (Ethanol was used as a mutual diluent.) The resulting solutions were refluxed at temperatures in the range of 130-195°C for 2 h. After refluxing, much of the solvent was evaporated (to remove residual propanol and residual "acacH") and then ethanol was added back to the sol (ethanol/Zr molar ratios in the range of ~100-200). The refluxed Zr-containing precursors were partially hydrolyzed (at 50°C for 2 h) using acidic conditions (HNO_3/Zr molar ratios in the range of 0.04-0.27) and an H_2O/Zr molar ratio of 24. Glycerol ($C_3H_8O_3$, Fisher Scientific, Fair Lawn, NJ) or phenol-formaldehyde resin ("novolac" type, Georgia Pacific, Atlanta, GA) were added to some solutions to increase the C/Zr ratio in the powders used for carbothermal reduction. Glycerol additions were made directly to refluxed solutions (i.e., prior to hydrolysis) using glycerol/Zr molar ratios in the range of 0.17-0.63. In contrast, phenolic

resin was added to hydrolyzed solutions as an ethanol-based solution at a 1:1 molar ratio of C:Zr. Hydrolyzed solutions were initially concentrated by rotary evaporation and then dried to powders at 120°C (2 h).

The dried powders were subsequently pyrolyzed at temperatures in the range of 800-1100°C (1-2 h) in a flowing argon atmosphere to produce carbon/zirconia mixtures. The C/Zr ratios in some of the pyrolyzed (1100°C, 1 h) samples were determined from weight losses that occurred upon further heat treatment (1100°C, 1 h) in air (i.e., in order to remove carbon by oxidative combustion). Sample weight losses during argon pyrolysis and oxidative combustion were also monitored in-situ using thermal gravimetric analysis, TGA (Model STA 409, Netzsch, Exton, PA). Pyrolyzed powders were subsequently heat treated at temperatures in the range of 1200-1800°C (2 h) in flowing argon. Selected heat-treated samples were characterized for weight loss, phase development, chemical composition, and crystallite size.

X-ray diffraction, XRD (Model PW1800, Philips Analytical, Netherlands), was used to determine the phases present and the ZrC lattice parameters in selected powder samples. In addition, ZrC and ZrO_2 crystallite sizes were calculated from the broadening of the XRD peaks using the Scherrer equation.[28] Selected pyrolyzed and carbothermally-reduced powders were analyzed for carbon and/or oxygen content based on analysis of the CO_2 evolution during oxidative combustion (Sherry Laboratories, Muncie, IN; LECO Corp., St. Joseph, MI).

The sintering behavior was evaluated using a ZrC-based powder prepared by carbothermal reduction at 1475°C. The powder was milled for 10 minutes to break up aggregates using a Spex mill (Model 8000, Spex Certiprep, Metuchen, NJ). The milled powder was mixed with approximately 10 vol% organic binder (polyvinyl alcohol/polyethylene glycol mixture) and dry pressed at ~250 MPa using a steel die with a cylindrical cavity. The binder was removed by heat treatment at 1150°C (1 h in argon). All samples were initially "pre-sintered" at 1600°C (2 h in argon) and then subsequently sintered at temperatures in the range of 1725-1950°C (2 h in argon). The bulk densities of the samples were

determined based on the weight and geometric dimensions of the cylinder-shaped samples. In addition, the bulk density and open porosity were determined for some samples using the Archimedes displacement method with distilled water as the suspending liquid. Relative (percentage) densities were calculated using a solid ("true") density value that was determined from the XRD lattice parameter measurement.

3.1.3 Hafnium Carbide (HfC)

The starting material for HfC synthesis was hafnium tetra-chloride ($HfCl_4$, Alfa AESAR, Ward Hill, MA). This was used to synthesize hafnium tetra-isopropoxide, $Hf(OC_3H_7)_4$, following procedures in the literature.[29,30] The hafnium isopropoxide was mixed with a large excess of "acacH" (i.e., Hf propoxide/"acacH" molar ratios in the range of 0.020 - 0.033) with reagent-grade (Fisher Scientific, Suwanee, GA) propanol/benzene solutions as a mutual diluent. Mixed solutions were refluxed at temperatures in the range of 145-155°C for 4 h. After refluxing, most of the solvent was evaporated (to remove residual "acacH," propanol, and benzene) and then ethanol was added back to the sols (ethanol/Hf molar ratios in the range of 400-500). The Hf-containing precursors were then hydrolyzed at 45°C (1 h) under acid conditions using an H_2O/Hf molar ratio of 16 and HNO_3/Hf molar ratios in the range of 0.18 - 1.54). It should be noted that a secondary soluble carbon source was *not* added to any of metal-organic solutions, either prior to or after the hydrolysis/condensation step. Solutions were then given the various heat treatment steps (i.e., solvent evaporation/drying, pyrolysis, and carbothermal reduction) in the same manner as described for the ZrC synthesis.

The synthesized products were characterized using the same methods described earlier. In addition, some Hf-based solutions and powders were characterized by Fourier transform infrared spectroscopy, FTIR (Model Nexus 870, Nicolet Instrument Corp., Madison WI). An as-synthesized hafnium propoxide solution was concentrated (~84 wt% propoxide solution) and subsequently loaded (under inert atmosphere) into a KBr liquid cell for FTIR analysis. A sample refluxed with "acacH" was concentrated (~4 wt% solution) and subsequently deposited onto a porous KBr powder compact.

Vacuum was then applied to the solution-infiltrated compact to remove most of the solvent prior to FTIR analysis. An Hf-based powder produced after the hydrolysis, concentration, and drying steps was mixed with KBr powder and pressed into a compact for the FTIR analysis. (The two samples prepared with KBr powder had exposure to the ambient air atmosphere, so some adsorbed moisture was present in the compacts.)

3.2 Silicon Carbide (SiC)

The starting materials used to produce the fine-scale silica/carbon mixtures for the carbothermal reduction reaction were tetraethoxysilane (TEOS, $[Si(OC_2H_5)_4]$, Alfa Aesar, Ward Hill, MA) and a phenol-formaldehyde resin ("novolac" type, Georgia Pacific, Atlanta, GA). Ethanol was used as a mutual solvent. The processing conditions were selected to promote nanometer-scale mixing: (i) The phenolic resin was comprised of low-molecular-weight oligomers ($M_n < 2000$). (ii) The TEOS was processed using acidic conditions (HNO_3/TEOS molar ratio of 0.01) and relatively low water content (H_2O/TEOS molar ratio of ~ 2). These conditions are known to produce polysilicate species with fine size (~ 5 nm or less).[31]

Mixed TEOS/phenolic resin solutions were initially heated at 65°C for 1-5 hr. Sols were then slowly concentrated at $\sim$35-55°C by rotary evaporation. The sol viscosity continually increased as the liquid was evaporated and eventually an immobile gel was formed. Gels were vacuum dried at low temperature ($\sim$40-70°C) for at least 36 h to ensure removal of all solvent and to produce a porous, brittle material. The dried material was gently crushed and ground using an agate mortar and pestle. The ground material was sieved (140 mesh size) to produce a free-flowing powder with relatively coarse size. The sieved powder was pyrolyzed at 1100°C (2-4 h) in a flowing argon atmosphere. This resulted in the removal of volatile decomposition products from the precursor materials and the development of fine-scale silica/carbon mixtures. The pyrolyzed samples were then heat treated in the range of 1160-1495°C in flowing argon in order to carry out the carbothermal reduction reaction to produce SiC. The weight

losses resulting from these heat treatments were recorded. The samples used to investigate the carbothermal reduction reaction had initial C/Si molar ratios (i.e., after pyrolysis) of 2.4 and 4.6.

Powder samples were characterized by X-ray diffraction, XRD (Model PW1800, Philips Analytical, Netherlands) to determine the phases present after heat treatment. The SiC crystallite sizes were calculated from the broadening of the XRD peaks using the Scherrer equation.[28] The gas adsorption/condensation method (Model ASAP 2000, Micromeritics, Norcross, GA) was used to determine the powder porosity characteristics. The carbon contents for pyrolyzed and carbothermally-reduced powders were determined from analysis of the evolved gas from oxidative combustion (Sherry Laboratories, Muncie, IN). Energy dispersive X-ray spectroscopy, EDX (Model 3600-0398, Kevex X-ray, Foster, CA) was used for semi-quantitative elemental analysis of deposits that were formed on substrates located downstream from the powder reaction mixtures.

4.0 RESULTS AND DISCUSSION

4.1 Zirconium Carbide (ZrC)

An idealized reaction to produce stoichiometric ZrC by carbothermal reduction (CTR) involves reacting carbon and zirconia in a 3:1 molar ratio:

$$3C_{(s)} + ZrO_{2(s)} = ZrC_{(s)} + 2CO_{(g)} \quad (1)$$

In this study, powders with different C/ZrO_2 ratios were prepared by varying the solution synthesis conditions. For example, Fig. 2 shows that C/Zr molar ratios in pyrolyzed samples (1100°C, 1 h) were varied in the range of ~1.6 to ~2.4 by changing the HNO_3/Zr molar ratio (from 0.12 to 0.42, respectively) during solution synthesis. (In these experiments, the Zr propoxide/"acacH" molar ratio used in the refluxing step (at 195°C) was 0.33 and the H_2O/Zr ratio used in the hydrolysis/condensation step was 24.) Samples with higher C/Zr molar ratios were produced using solutions with glycerol or phenolic resin additions. Fig. 3 shows that samples with C/Zr molar ratios in the range of ~2.4 to ~3.5 were prepared by using glycerol/Zr molar ratios in the range of 0 to 0.63, respectively, during solution synthesis. (The HNO_3/Zr molar ratio was 0.27 and the "acacH" and water concentrations were the same as used for the samples in Fig. 2.) Figure 4 shows a typical TGA plot of residual weight vs. temperature for a solution-derived powder (dried at 120°C, 2h) which was heated (in argon) to 1100°C and held at temperature for 1 h. (The sample was prepared using molar ratios of 0.25 for Zr propoxide/"acacH," 0.04 for HNO_3/Zr, and 24 for H_2O/Zr. Phenolic resin was added at a C/Zr molar ratio of 1.0.) Figure 4 shows that pyrolytic decomposition of the mixed precursor was mostly completed by ~550°C, although small weight losses were observed throughout the rest of the heat treatment. (There was also a small weight loss of ~0.4% observed during the 1 h hold at 1100°C.)

Figure 5 shows X-ray diffraction (XRD) results for as-dried (120°C) and heat treated samples (2 h at 800-1400°C in argon) prepared from the same powder that was used for the TGA experiment in Fig. 4. The as-dried powder was amorphous. The XRD pattern for a sample pyrolyzed at 800°C (2 h)

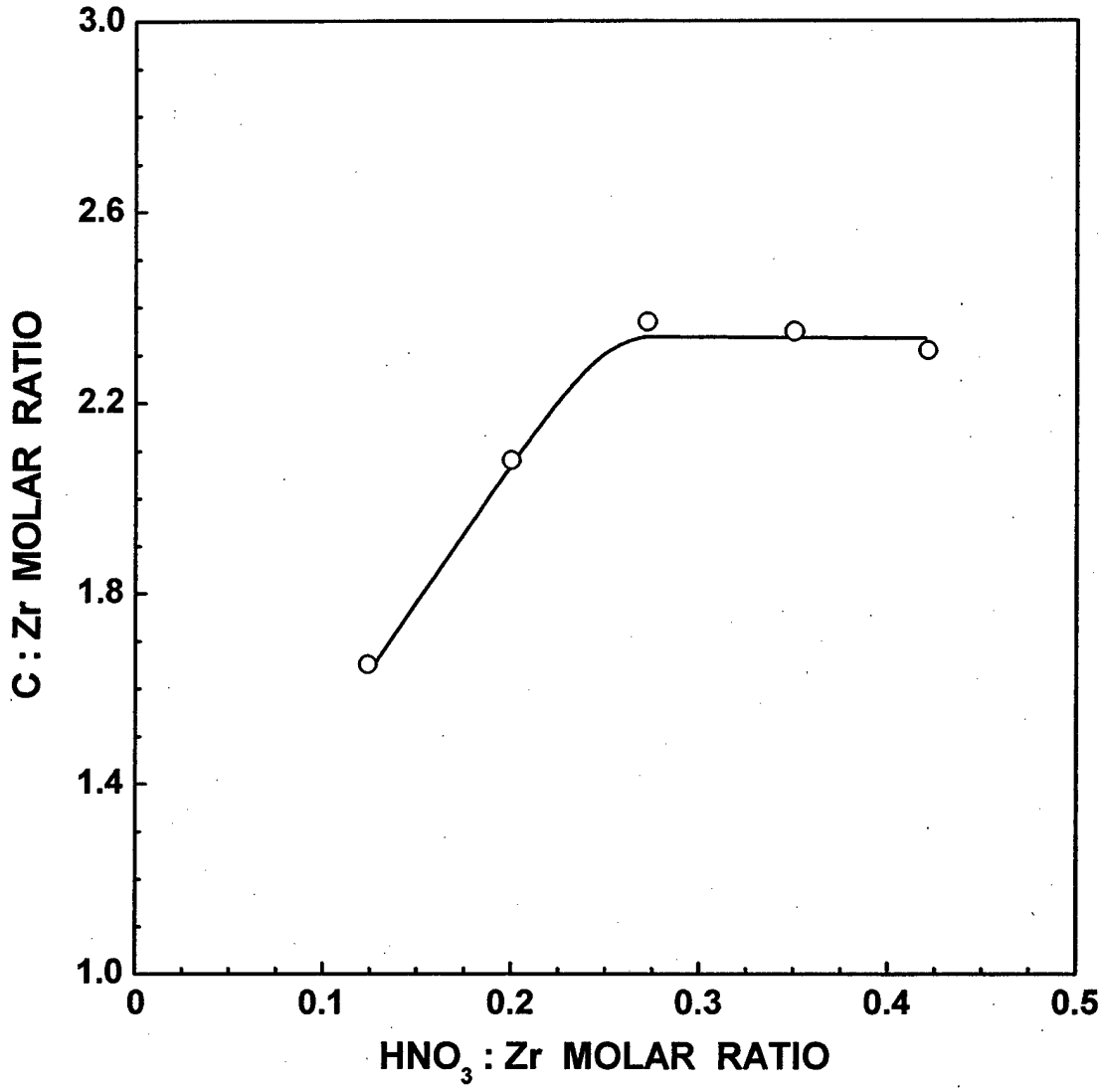

Fig. 2. Plot of C/Zr molar ratio in pyrolyzed (1100°C, 1 h) samples that were prepared using varying HNO_3/Zr molar ratios during solution synthesis.

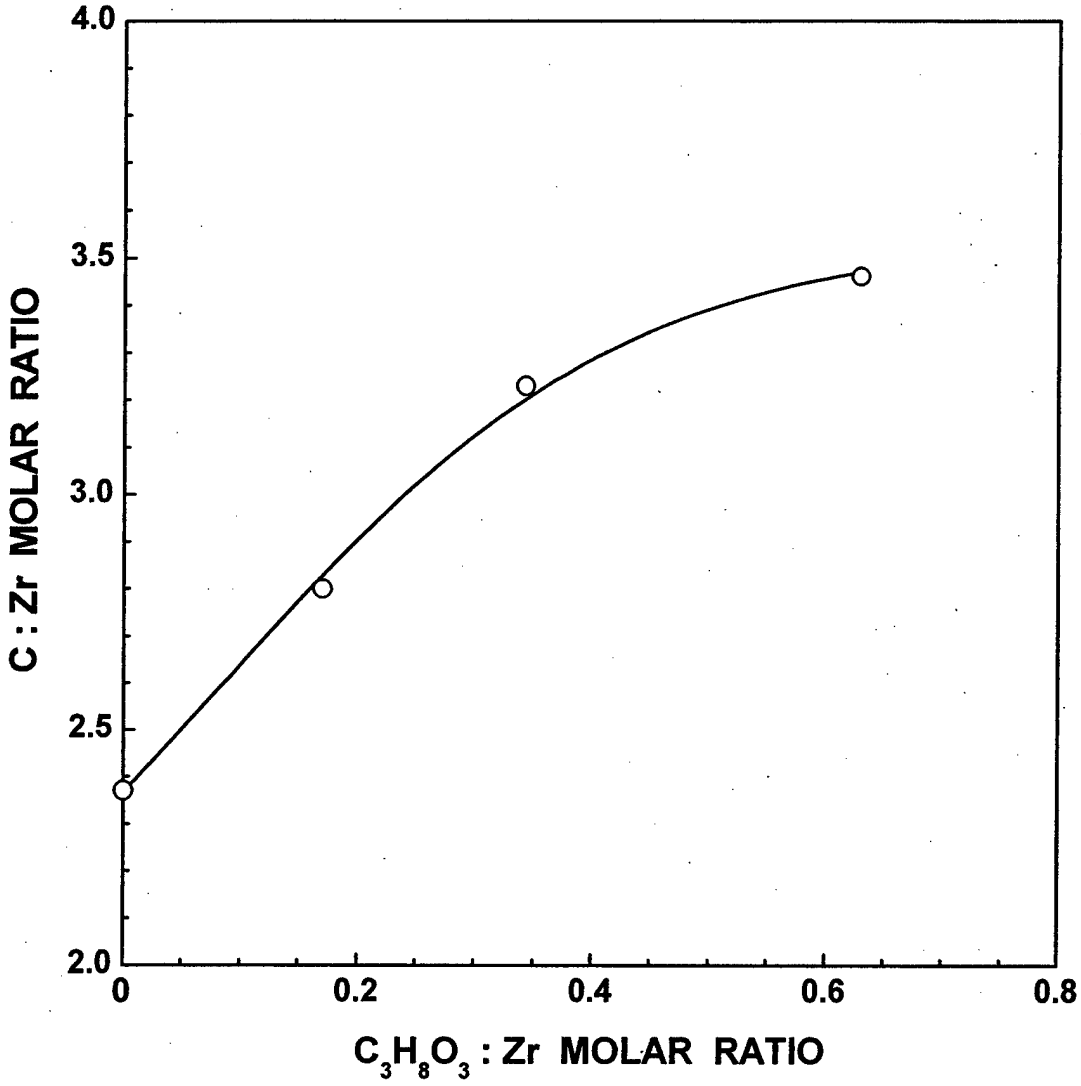

Fig. 3. **Plot of C/Zr molar ratio in pyrolyzed (1100°C, 1 h) samples that were prepared using varying glycerol/Zr molar ratios during solution synthesis.**

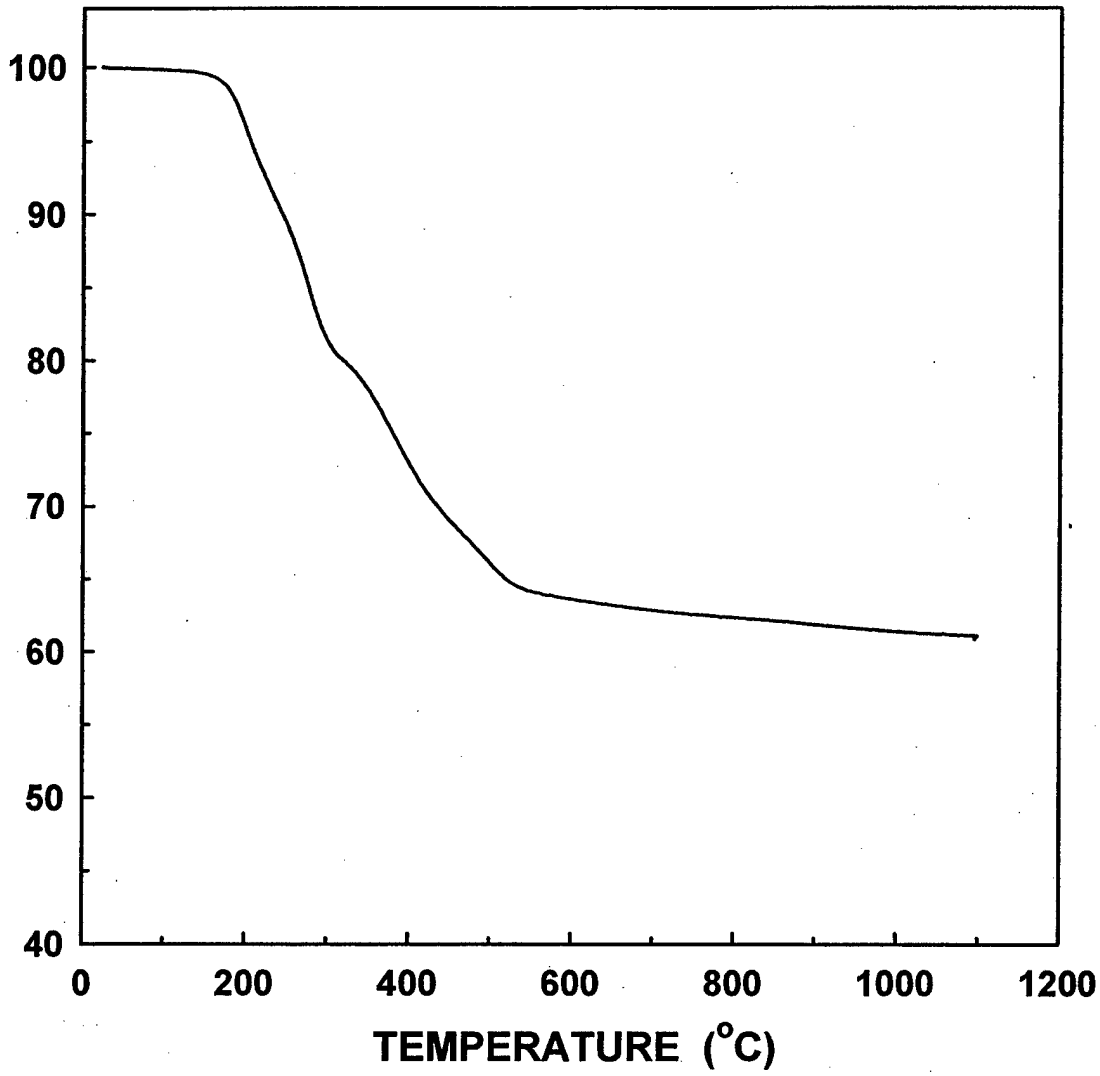

Fig. 4. **TGA plot of weight loss vs. temperature for an as-dried (120°C) precursor prepared from a (zirconium n-propoxide/phenolic resin)-based sol.**

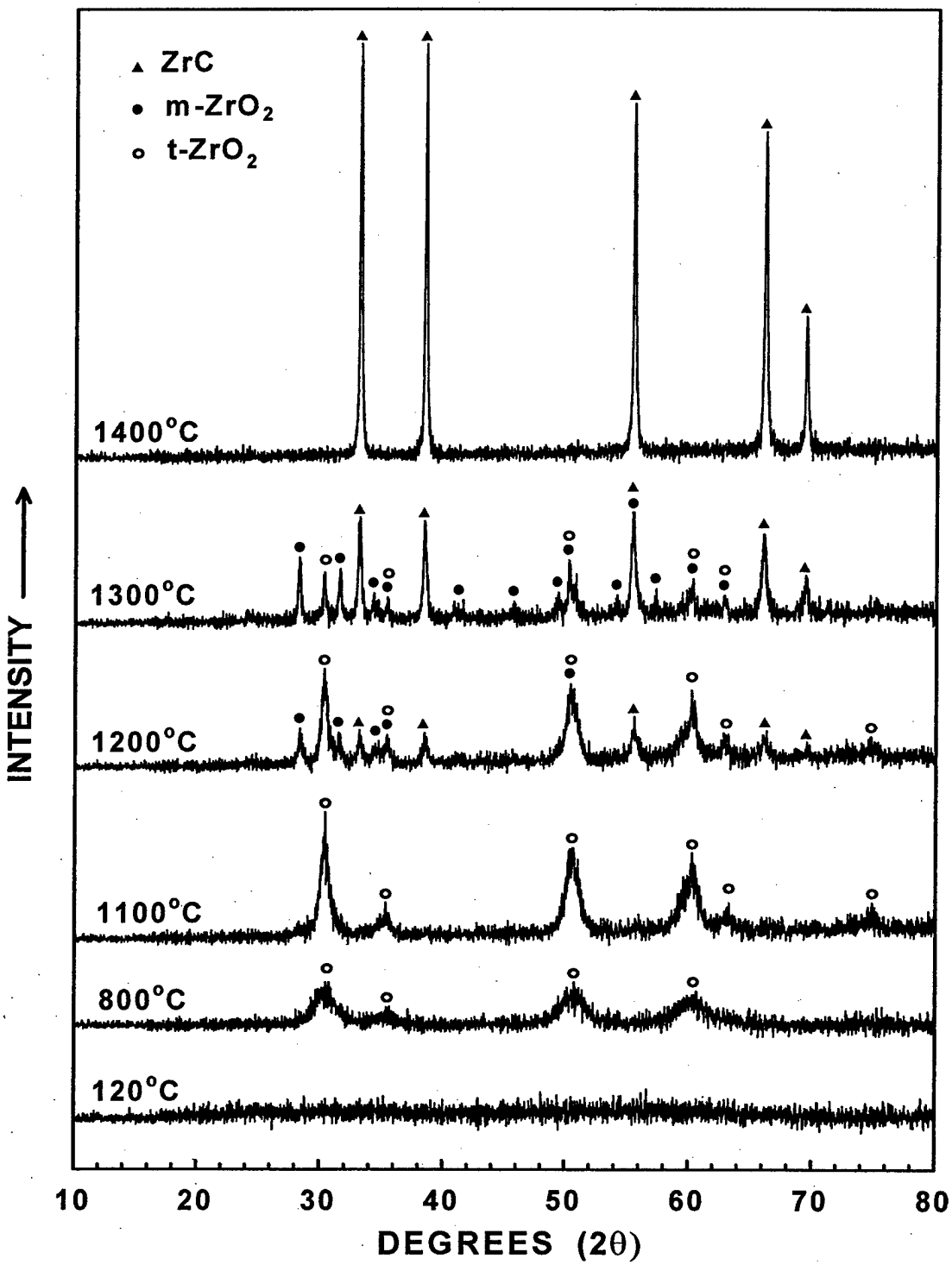

Fig. 5. X-ray diffraction patterns for as-dried (120°C) and heat treated (800-1400°C) samples prepared from a (zirconium n-propoxide/phenolic resin)-based sol.

shows weak and broad diffraction peaks that are due to tetragonal zirconia (t-ZrO_2). The carbon present in the sample remained amorphous. The only significant change in the XRD pattern for a sample heat treated at 1100°C (2 h) is that the t-ZrO_2 peaks increased in intensity.

The initial formation of ZrC was observed in the sample that was heat treated at 1200°C (Fig. 5). The XRD pattern for this sample also shows that some t-ZrO_2 had transformed to monoclinic ZrO_2 (m-ZrO_2). ZrC became the predominant phase after heat treatment at 1300°C, although a substantial amount of m-ZrO_2 and t-ZrO_2 were still present. ZrC was the only crystalline phase observed in the samples heat treated at 1400°C (Fig. 5) and at higher temperatures (not shown in Fig. 5). However, characterization results described below (i.e., measurements of weight loss, carbon and oxygen contents, and lattice parameter) show that the 1400°C sample was *not* phase-pure stoichiometric ZrC. Instead, the sample consisted of "zirconium oxycarbide" (i.e., ZrC with some oxygen dissolved in the lattice) and some residual amorphous carbon.

Table 1 shows the carbon and oxygen contents for samples prepared from the same powder used in the TGA and XRD experiments (Figs. 4 and 5). A sample pyrolyzed at 1025°C (2 h) had a carbon content of 23.3 wt%. (This is equivalent to a C/Zr molar ratio of 3.1, i.e, assuming that the pyrolyzed material contained only ZrO_2 and C.) Table 1 also shows that subsequent heat treatment at 1475°C (2 h) produced a sample with 13.4 wt% carbon. This carbon content is greater than the value of 11.6 wt% that would be expected if the sample was phase-pure stoichiometric ZrC. Hence, it is apparent that the sample retained some free carbon (XRD-amorphous) after the heat treatment. Furthermore, the sample also contained 3.3 wt% oxygen. Since ZrO_2 is not observed in XRD patterns for samples heat treated at or above 1400°C, it is evident that the oxygen present in the sample was dissolved in the zirconium carbide lattice.

Table 1 also shows that further heat treatment at 1800°C (2 h) produced a sample with carbon concentration (11.3 wt%) equivalent to that of stoichiometric ZrC (i.e., within experimental error of the measurement). In addition, the oxygen content was reduced to a very low level (0.1 wt%). The decrease

Table 1. Chemical Analysis and Lattice Parameter Values of ZrC Powders

Processing Temperature (°C)	Carbon Concentration (wt%)	Oxygen Concentration (wt%)	Lattice Parameter (nm)
1025	23.3	n.d.	n.d.
1300	n.d.	n.d.	0.4694
1400	n.d.	n.d.	0.4691
1475	13.4	3.3	0.4691
1800	11.3	0.1	0.4696

in carbon and oxygen contents for the 1800°C sample is consistent with weight loss behavior that was observed (see Fig. 6) when 800°C-pyrolyzed powder was heat treated at temperatures in the range of 900-1800°C for 2 h. Figure 6 shows that there was still a significant weight loss upon heat treatment above 1400°C, even though samples heat treated at (or above) this temperature showed no residual ZrO_2 in the XRD patterns (Fig. 5). In combination, the weight loss (Fig. 6) and the decrease in carbon and oxygen contents (Table 1) upon heat treatment to 1800°C can be explained by a carbothermal reduction reaction in which the reactants were zirconium oxycarbide and free carbon:

$$ZrO_yC_{(1+y-x)\,(s)} + xC_{(s)} = ZrC_{(s)} + yCO_{(g)} \quad (2)$$

The present study is consistent with previous studies which have shown that there is considerable solid solubility of ZrO_2 in ZrC.[10,32-34] The ZrC (face-centered cubic) lattice parameter decreases with increasing amount of dissolved oxygen.[10,32-34] Table 1 shows the ZrC lattice parameters for samples prepared in this study. The lattice parameter was 0.4694 nm for the 1300°C sample. The value decreased to 0.4691 nm for the ZrC in the 1400°C and 1475°C samples. This indicates that either some zirconia dissolved in the ZrC lattice as the heat treatment temperature was increased (from 1300°C to 1475°C) or that direct formation of an oxycarbide composition (instead of stoichiometric ZrC) was more favorable at the higher reaction temperatures (i.e., at 1400°C and 1475°C). With further heat treatment at 1800°C, the ZrC lattice parameter increased to 0.4696 nm. This result is again consistent with the reaction shown in equation (2) in that the lattice parameter increased to a value that is expected for near-stoichiometric ZrC.[32-34]

Figure 7 shows the average crystallite sizes (determined by XRD measurements on the same samples shown in Fig. 5) for each phase (ZrC, t-ZrO_2, and m-ZrO_2) as a function of heat treatment temperature. The t-ZrO_2 crystallites remain relatively small (<20 nm) in the pyrolyzed samples (800-1100°C). Rapid crystallite growth begins with the onset of the carbothermal reduction reaction above1100°C. The crystallite sizes for both the t-ZrO_2 and m-ZrO_2 phases increased from ~30-45 nm at 1200°C to ~110-130 nm at 1350°C. The ZrC crystallites also increased from ~40 nm in the early stages

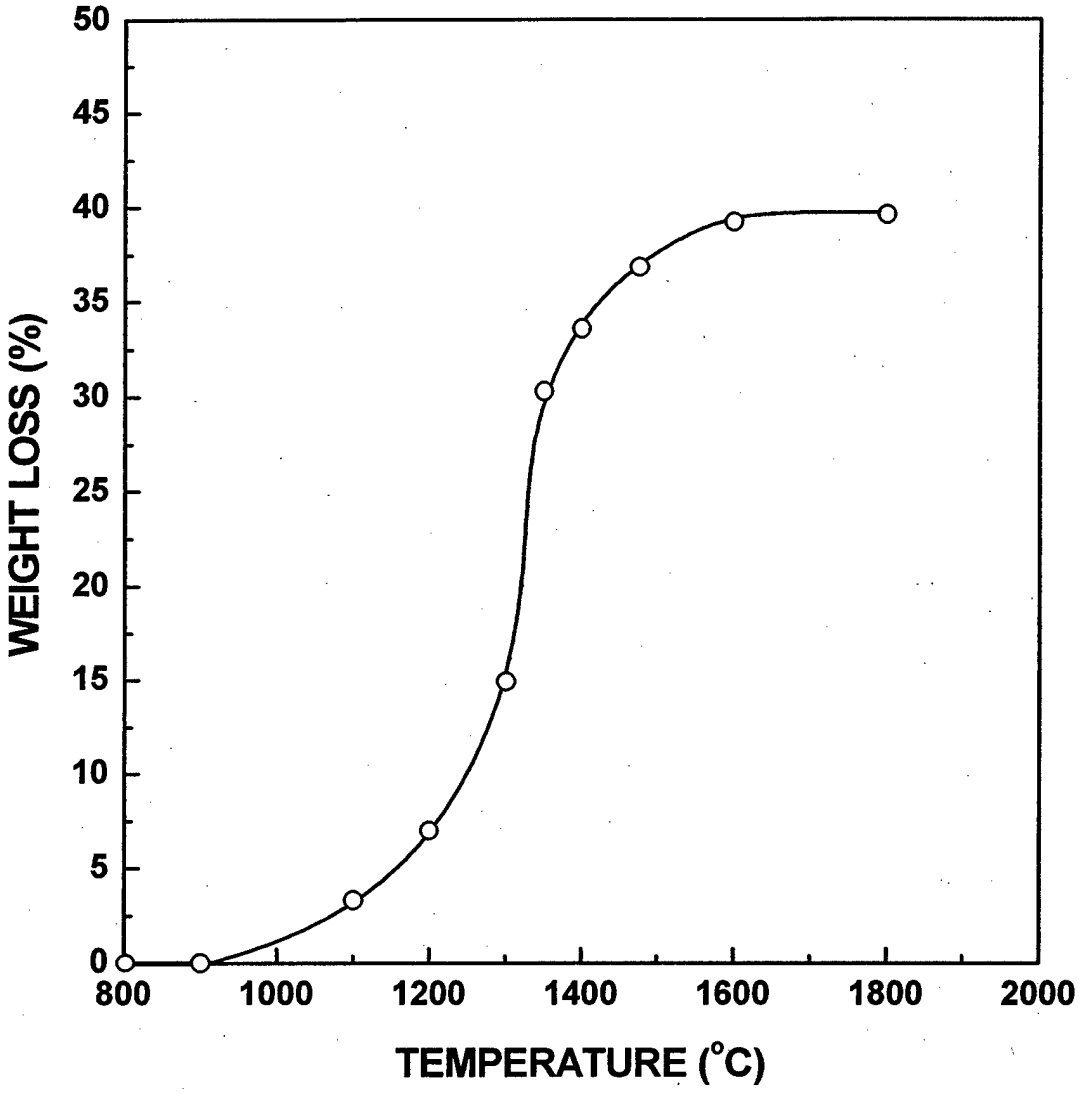

Fig. 6. Plot of weight loss vs. temperature for an 800°C-pyrolyzed sample prepared from a (zirconium n-propoxide/phenolic resin)-based sol.

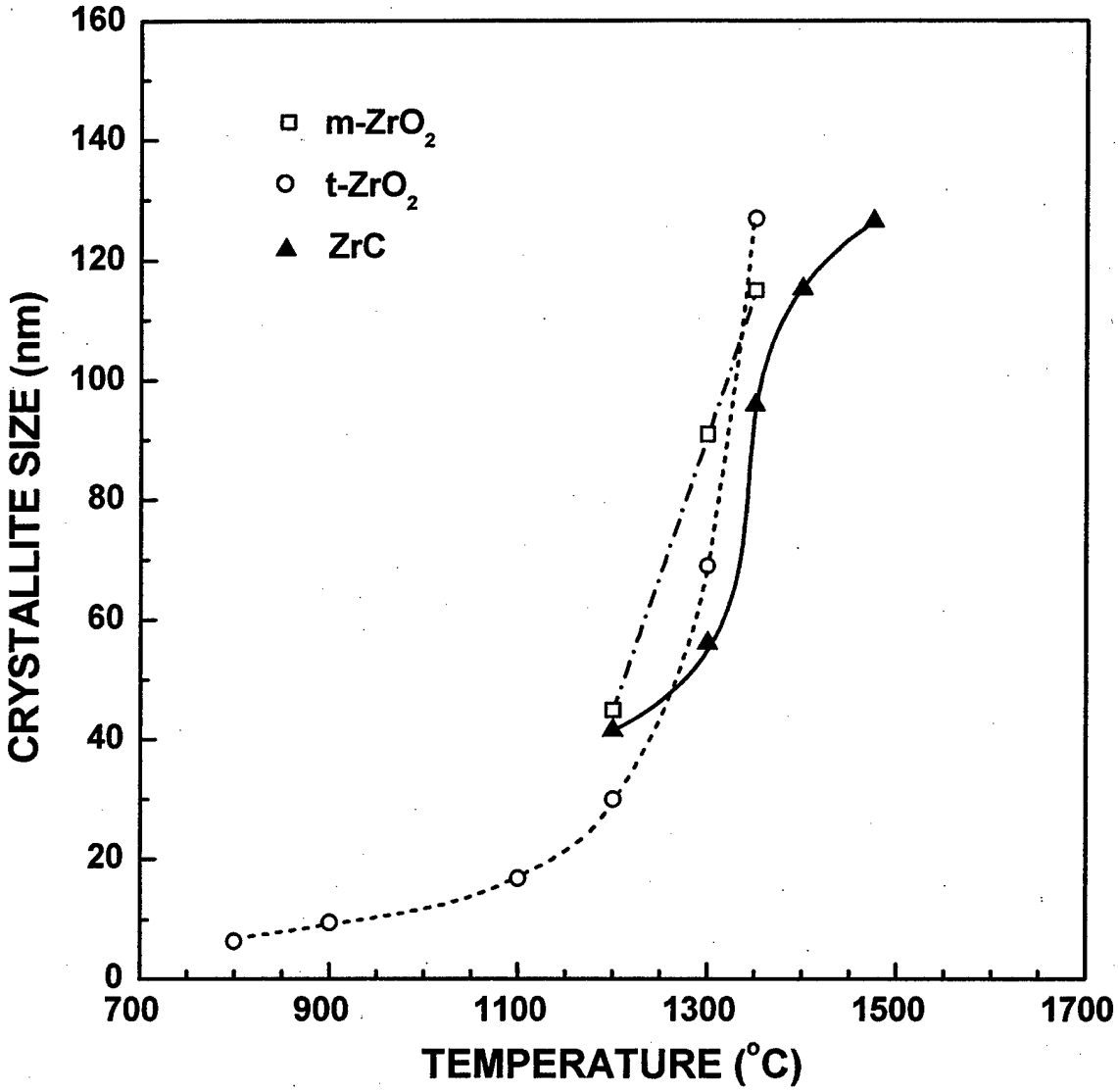

Fig. 7. Plots of the t-ZrO_2, m-ZrO_2, and ZrC crystallite sizes (determined from XRD line broadening measurements) vs. heat treatment temperature.

of the reaction (1200°C sample) to ~120 nm in the 1400°C sample (which contained no ZrO_2 second phase). The close correspondence in crystallite size growth for the ZrC and two ZrO_2 phases is consistent with certain aspects of the reaction mechanism suggested by Maitre et al.[34] in a carbothermal reduction study carried out using mixtures of ZrO_2 and C powders. In particular, they proposed that the transformation proceeded by the "contracting volume" mechanism in which growth of ZrO_xC_y proceeds from the surface to the interior of the ZrO_2 particles.

The densification behavior was investigated using a powder which had a slightly carbon-deficient composition (relative to stoichiometric ZrC) after sintering. The powder was prepared using molar ratios of 0.33 for Zr propoxide/"acacH," 0.27 for HNO_3/Zr, and 24 for H_2O/Zr. The "acacH" refluxing temperature was 195°C. Phenolic resin was added at a C/Zr molar ratio of 1.0. The heat treatment conditions for pyrolysis and carbothermal reduction were 800°C (2 h) and 1475°C (2 h), respectively. The reacted powder was milled for 10 min prior to dry pressing. The XRD pattern for this powder showed ZrC as the only crystalline phase. The crystallite size determined by XRD line broadening measurements was ~100 nm. The powder surface area was 17 m^2/g. (This surface area is equivalent to a particle size of 57 nm if the particles were non-contacting, non-porous, monosized spheres with true solid density of 6.6 g/cm^3.) Dry-pressed powder compacts had a relative "green" density of ~44% after pyrolysis of the organic binder at 1150°C (2 h). (The powder density used for the relative density calculation was 6.6 g/cm^3.)

Figure 8 shows a plot of the sample bulk density vs. sintering temperature. The bulk densities reported in this figure were calculated from the sample weight and geometric dimensions. The bulk density and open porosity were also determined by the Archimedes displacement method for the samples sintered at 1900°C and 1950°C. The bulk density measurements for the two methods gave similar values; the values for the geometric vs. Archimedes measurements were 6.50 vs. 6.53 g/cm^3, respectively, for the 1900°C samples and 6.53 vs. 6.54 g/cm^3, respectively, for the 1950°C samples. The 1900 and 1950°C samples both showed zero open porosity from the Archimedes measurement method.

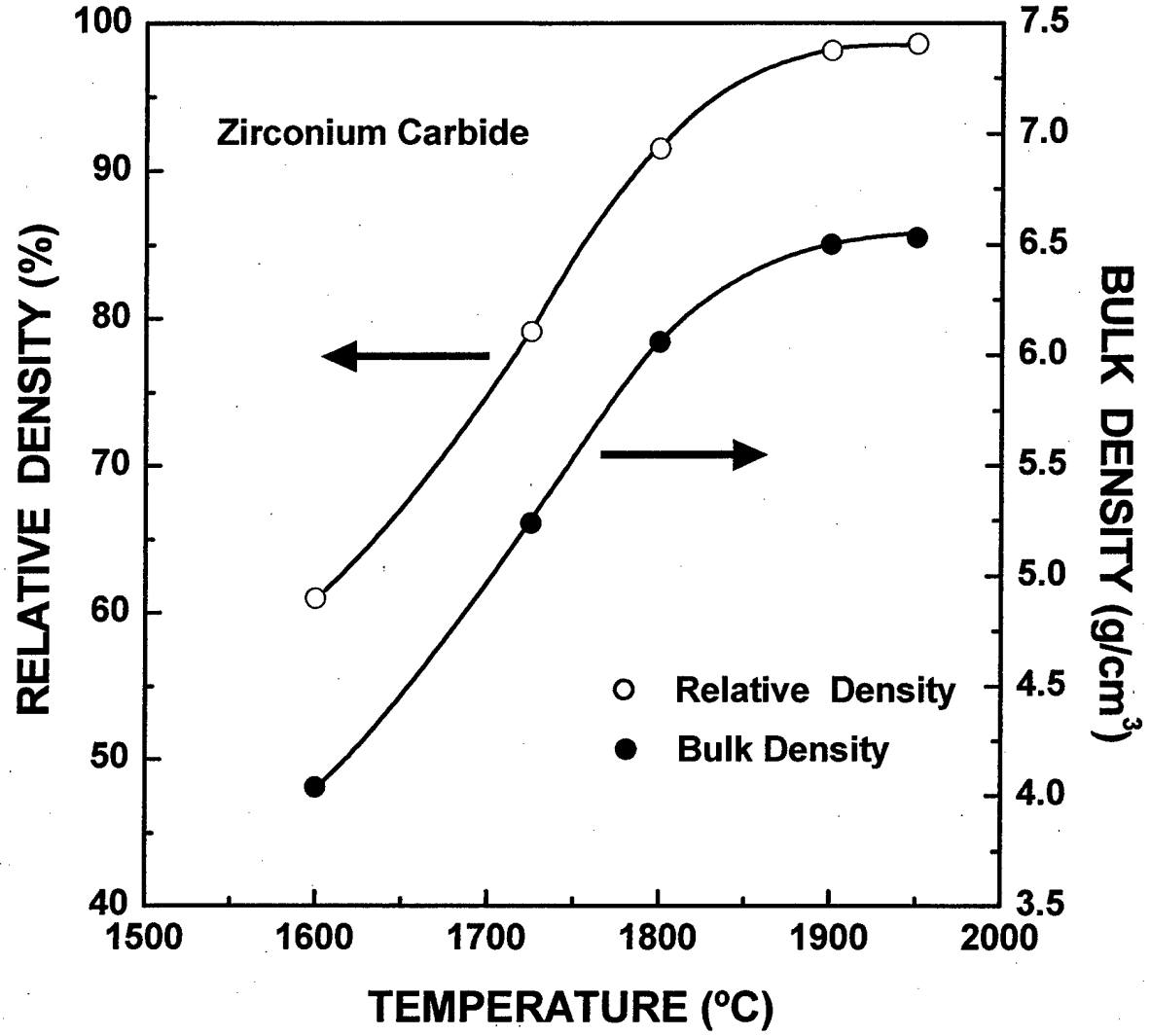

Fig. 8. **Plots of relative density and bulk density vs. sintering temperature for dry-pressed ZrC powder compacts.**

Figure 8 also shows a plot of the relative density vs. sintering temperature for the samples. The relative densities were ~92%, ~98%, and ~99% for the samples sintered at 1800°C, 1900°C, and 1950°C, respectively. The relative densities for all the sintered (1600-1950°C) samples were calculated by assuming that the solid true density was 6.62 g/cm^3. The latter value was based on using the lattice parameter measured on a powder sample which had been heat treated at 1900°C (2 h) and by assuming that the sintered samples were 100% stoichiometric ZrC. In fact, samples sintered at the lower temperatures probably still had some dissolved oxygen in the ZrC lattice. (Some free carbon may have been present also.) In addition, the samples sintered at the higher temperatures were somewhat deficient in carbon relative to stoichiometric ZrC. The carbon contents measured on powder samples heat treated at 1800°C (2 h) and 1900°C (2 h) were 11.0 and 10.8 wt%, respectively. Hence, the solid true densities for the samples probably varied with sintering temperature (from 1600 to 1950°C). Nevertheless, the values are not expected to be significantly different from the assumed value of 6.62 g/cm^3.

The maximum sintered densities obtained in this study were equal to or higher than the values reported in previous studies of ZrC sintering. In addition, the sintering temperatures (1900-1950°C) were lower. Nezhevenko et al., Bulychev et al., and Lanin et al. reported pressureless sintering of ZrC to maximum relative densities of 97-98% using temperatures in the range of 2400-2600°C.[35-37] Barnier et al.[38] also reported maximum relative densities of ~97% and ~98% by hot pressing at 2000°C (2 h) and 2300°C (1 h), respectively, with an applied pressure of 40 MPa.

4.2 Hafnium Carbide (HfC)

Figure 9 shows FTIR spectra for (a) concentrated (~84 wt%) hafnium propoxide solution, (b) dried sample prepared after refluxing the hafnium propoxide solution with excess "acacH," and (c) dried powder prepared after hydrolysis of the "acacH"-refluxed solution. The spectrum for the hafnium propoxide is in good agreement with results reported by Lynch et al.[39] (The latter researchers produced hafnium propoxide by the same method used in the present study, i.e., by reacting $HfCl_4$ with

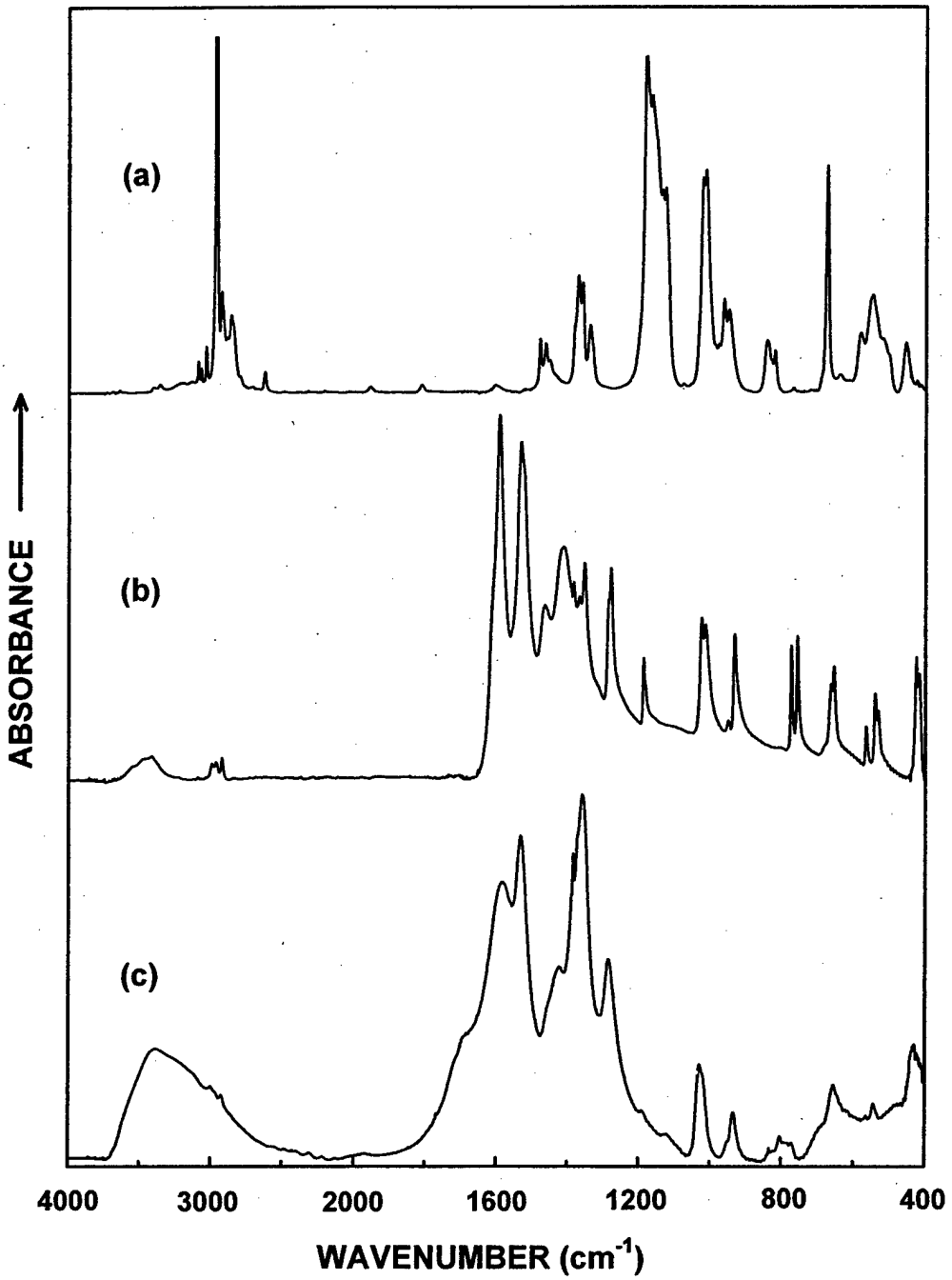

Fig. 9. **FTIR spectra for (a) concentrated hafnium propoxide solution, (b) dried sample prepared after refluxing the hafnium propoxide solution with acetylacetone, and (c) dried powder prepared after hydrolysis of the acac-refluxed solution.**

isopropanol.) Figure 9(a) contains some additional peaks (i.e., besides those associated with hafnium propoxide) due to the solvent components in the concentrated solution (i.e., benzene and isopropanol). Figure 9(b) shows the spectrum for a solution which was prepared by refluxing the hafnium propoxide solution at 155°C (4 h) with a large excess of "acacH" (i.e., molar ratio of 1:50). The propoxide was converted almost completely to hafnium 2,4 pentanedionate (i.e., "hafnium acac"). This is indicated by the close agreement of the spectral results shown in Fig. 9(b) with results reported by previous researchers [40,41] and by measurements (not shown in Fig. 9) that were carried out using a commercial source of "hafnium acac" (Strem Chemicals, Newburyport, MA).

As noted earlier, metal diketonates are usually more resistant to hydrolysis compared to the corresponding metal alkoxide. This provides an advantage in subsequent processing because it allows for better control over the C/Hf ratio that is subsequently obtained after the high temperature heat treatments. Fig. 9(c) shows the FTIR spectrum for the powder produced after hydrolysis, concentration, and drying of the "hafnium acac" solution. (The solution was prepared using molar ratios of $H_2O/Hf = 16$ and $HNO_3/Hf = 1.4$, respectively.) Hydrolysis of the "hafnium acac" precursor is indicated by the large, broad peak for the OH stretching vibration over the range of ~2700-3700 cm^{-1}. It is evident, however, that an extensive Hf-chelate structure is still present in the as-dried powder. For example, the strong symmetric and asymmetric stretching vibrations (at ~1595 cm^{-1} and ~1530 cm^{-1}, respectively) from C=O and C=C bonds in the chelate ring are still the most intense peaks in the spectra. Figure 9(c) also shows peak broadening has occurred in the hydrolyzed sample (e.g., in the ranges ~400-800 cm^{-1} and ~1200-1800 cm^{-1}) which presumably reflects the development of a more complex and disordered structure (i.e., compared to the "Hf acac"). Hydrolysis (and subsequent condensation) reactions result in partial replacement of Hf-O-C bonds (from the "Hf acac" structure) with Hf-OH bonds and Hf-O-Hf bonds. (The substantially amorphous character of this material was confirmed by XRD analysis on a similar dried powder.)

It was possible to produce heat-treated powders (pyrolyzed and carbothermally-reduced) with a

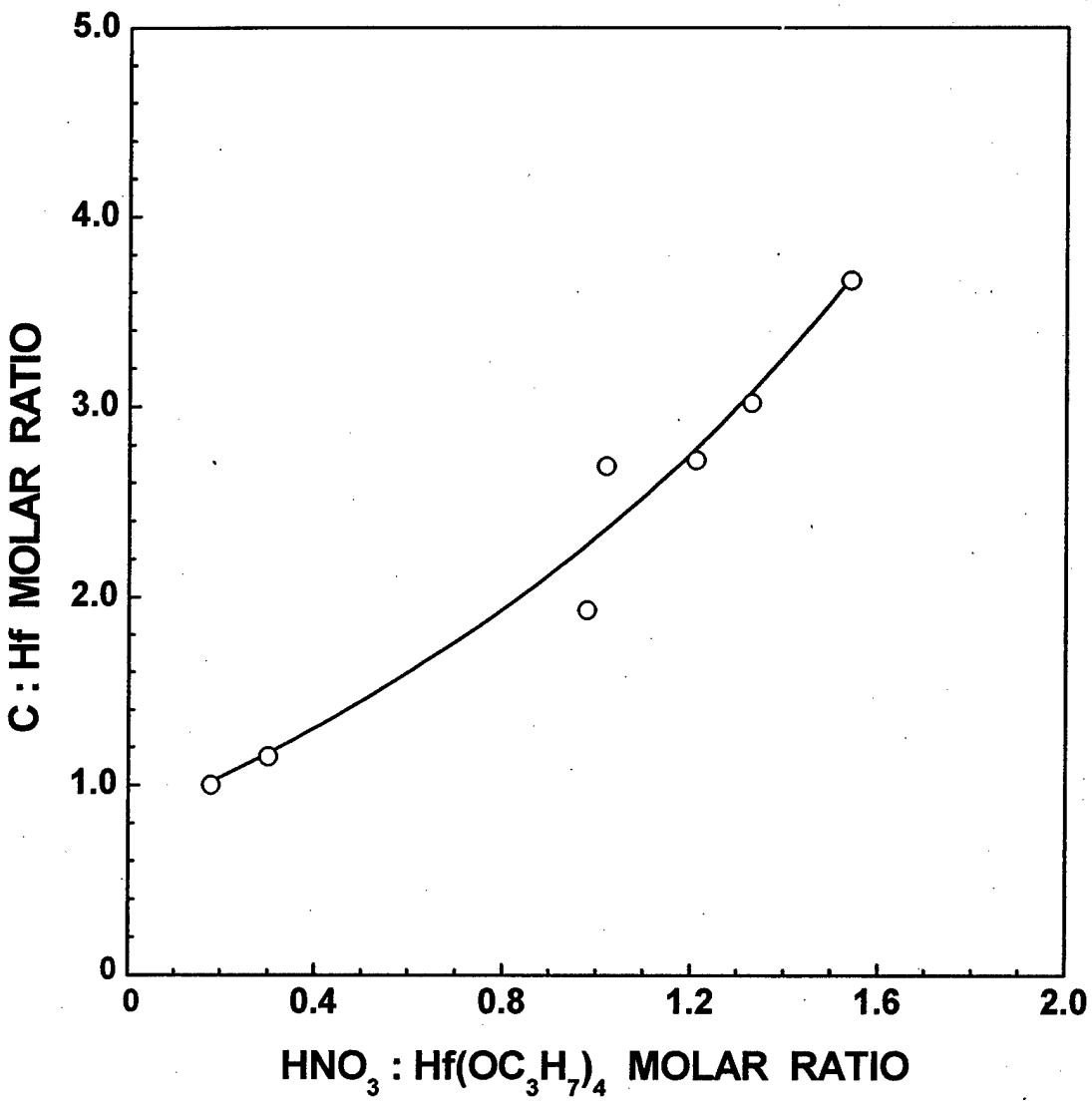

Fig. 10. **Plot of C/Hf molar ratio in pyrolyzed samples that were prepared using varying HNO_3/Hf molar ratios during solution synthesis.**

wide range of C/Hf ratios by using the fully chelated "Hf acac" compound as the starting material for the hydrolysis/condensation. The composition was varied by changing the acid and/or water concentrations used in the hydrolysis/condensation step. For example, Figure 10 shows the effect of acid concentration (i.e., HNO_3/Hf molar ratio) on the C/Hf molar ratio in pyrolyzed samples. (For these samples the Hf propoxide/"acacH" molar ratio used for refluxing (at 155°C) was 0.02 and the H_2O/Hf ratio used for hydrolysis/condensation was 16.) Figure 10 shows that pyrolyzed powders can be produced with a C/HfO_2 molar ratio of 3, i.e., the composition needed to produce stoichiometric HfC by carbothermal reduction. Note that this ratio was obtained without using a secondary source of soluble carbon (i.e., in contrast to the method used to produce the near-stoichiometric ZrC). Hence, near-stoichiometric HfC can be produced by using a "single-source" solution-based precursor.

Figure 11 shows TGA results for an as-dried (120°C) precursor which was heated (in flowing argon) to 1100°C and held at temperature for 1 h. (The sample was prepared using molar ratios of 0.02 for Hf propoxide/"acacH," 1.4 for HNO_3/Hf, and 16 for H_2O/Hf.) Pyrolytic decomposition of the dried precursor powder was mostly completed (~28 wt% loss) by ~600°C. A gradual weight loss of ~1.5 wt% occurred between 600-900°C and a more rapid weight loss of ~1.5 wt% occurred between 900-1025°C. The decomposition processes were essentially completed by 1050°C; there was no weight loss above this temperature (including during the 1 h hold at 1100°C). The product was a black powder. Heat treatment of this powder in air at 900°C for 1 h produced a white powder with a yield of 84.9%. (X-ray diffraction (XRD) analysis on a separate, but similar, sample showed that the oxidized product was monoclinic hafnium dioxide, m-HfO_2.) Thus, the original 1100°C-pyrolyzed product contained 15.1% carbon and a C/HfO_2 molar ratio of 3.1 (i.e., assuming that the pyrolyzed material contained only HfO_2 and C). Hence, the material was slightly carbon-rich compared to the ideal C/Hf molar ratio of 3 for producing stoichiometric HfC by a carbothermal reduction reaction analogous to the one shown in eq. (1) for ZrC.

Figure 12 shows XRD results for samples heat treated (in argon) in the range of 800-1600°C for

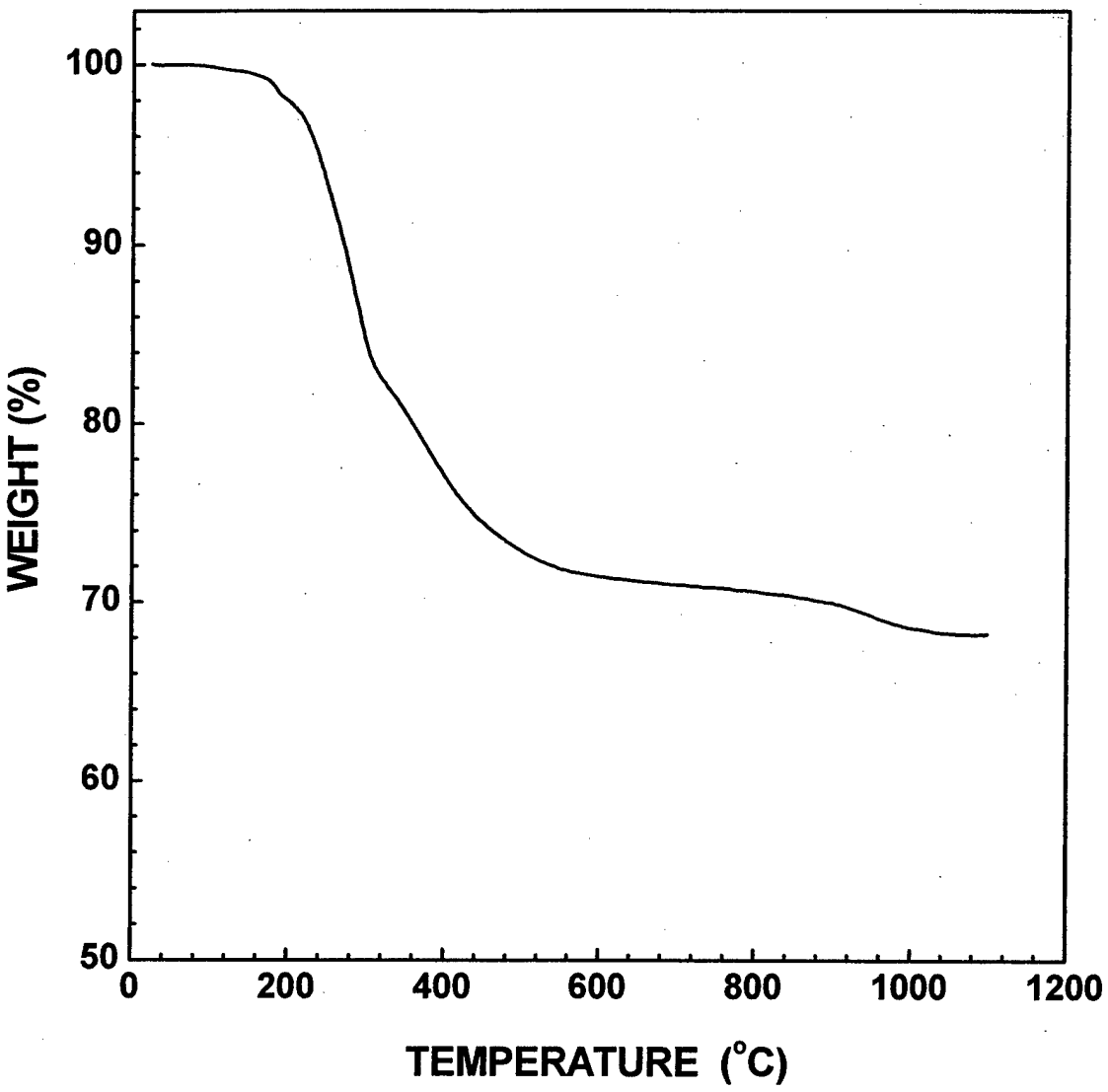

Fig. 11. TGA plot of weight loss vs. temperature for an as-dried (120°C) Hf-O-C precursor prepared by solution-based processing.

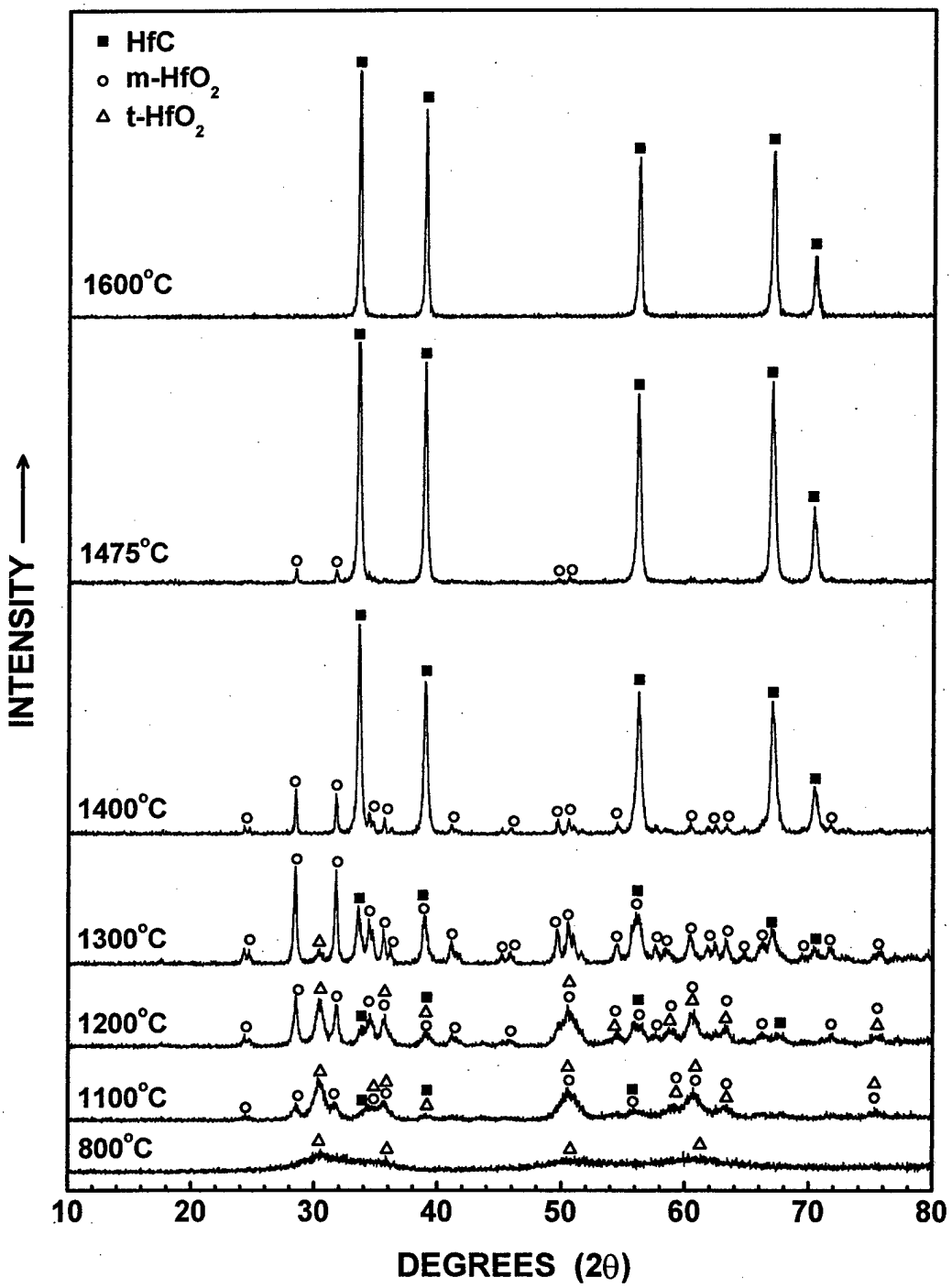

Fig. 12. X-ray diffraction (XRD) patterns for heat treated (800-1600°C) samples prepared from a solution-derived Hf-O-C precursor

sample was the tetragonal phase. Figure 12 shows that the t-HfO_2 became better crystallized after heat treatment at 1100°C. (Once again, it is difficult to rule out definitively the orthorhombic HfO_2 phase because of peak broadening.) The formation of some monoclinic hafnium oxide (m-HfO_2) was also observed in the 1100°C sample. In addition, the sample appeared to contain a trace of HfC (face-centered cubic).[46] It is difficult to be certain about the trace presence of HfC because the broad peaks from the HfO_2 phases would overlap with any weak HfC peaks that might be present. However, the XRD pattern for the 1100°C sample shows a very slight shoulder at the 2θ value ($\sim$33.4 degrees) for the most intense reflection for HfC (i.e., the (111) peak). Figure 12 shows that the peak intensities for the HfO_2 phases increased upon further heat treatment at 1200°C, especially for the monoclinic phase. The presence of a small amount of HfC is now clearly evident in the XRD pattern for this sample. The m-HfO_2 peak intensities continued to increase significantly in the 1300°C sample, while only a small amount of t-HfO_2 phase remained in the sample. The HfC peaks also increased in intensity significantly, although m-HfO_2 remained the primary crystalline phase. The phase development observed from 800°C to 1300°C in this study can be contrasted to the results reported by Kurokawa et al.[18] for samples heat treated in the range of 1000°C-1300°C. The XRD patterns for all their samples showed a single HfO_2 phase, with relatively broad diffraction peaks, that was very similar to the phase identified as t-HfO_2 in Fig. 12. The monoclinic phase was not observed at any heat treatment temperature in their study. In addition, only a trace of HfC was evident in their XRD pattern for a sample heat treated at 1300°C.

Figure 12 shows that a sample heat treated at 1400°C (2 h) consisted mostly of HfC. The amount of m-HfO_2 was reduced substantially compared to the 1300°C sample and no t-HfO_2 was present. The HfC peak intensities continued to increase for a sample heat treated at 1475°C and only a trace of m-HfO_2 was detected in the sample. HfC was the only crystalline phase detected in samples heat treated for 2 h at 1600°C (Fig. 12) and at 1800°C (XRD pattern not shown in Fig. 12). Although the 1475°C sample had only a small amount of HfO_2, several experimental observations indicated that the carbothermal reduction reaction still continued to a significant extent at the higher heat treatment temperatures, i.e., just as was

observed with the ZrC-based samples. First, there was significant weight loss at heat treatment temperatures above 1475°C. For example, the weight loss upon heat treatment from 1100°C to 1475°C was 17.6%, while the weight loss was 23.3% for heat treatment from 1100°C to 1800°C. (The latter value is close to the expected weight loss of 22.7% for the ideal HfC carbothermal reduction reaction.) Second, the overall carbon concentration for the 1475°C sample was 8.3 wt%. This value is significantly greater than the value of 6.3 wt% that would be expected if the sample was phase-pure stoichiometric HfC. Hence, it is apparent that the 1475°C sample retained some free carbon (XRD-amorphous) after the heat treatment. Third, a different sample (but with similar overall composition) was heat treated at 1500°C for 2 h and the measured oxygen content was 1.6 wt%. Essentially all of this oxygen must have been dissolved in the HfC lattice because HfO_2 was not observed at all in the XRD pattern for this sample. (This result is consistent with previous studies that have shown that there is considerable solid solubility of HfO_2 in HfC.[2,47]) Fourth, upon heat treatment at 1800°C, the overall carbon concentration decreased from 8.3 wt% for the 1475°C sample to 6.7 wt% for the 1800°C sample. Hence, the continued weight loss above 1475°C can be explained by the same type of carbothermal reduction reaction shown in eq. (2) in which "hafnium oxycarbide," (i.e., HfC with some oxygen dissolved in the lattice) reacts with excess carbon.

Figure 13 shows plots of the average crystallite sizes (determined by XRD measurements) for each phase (t-HfO_2, m-HfO_2, and HfC) as a function of heat treatment temperature. The t-HfO_2 crystallites that formed initially in the 800°C sample were only ~2.5 nm. The t-HfO_2 crystallite size increased gradually to ~15 nm as the heat treatment temperature increased to 1300°C. The m-HfO_2 crystallites were initially ~17 nm in the 1100°C sample and the size increased rapidly to ~75 nm in the 1400°C sample. This coincides with the period during which most of the carbothermal reduction reaction occurs. The HfC crystallites coarsen more gradually, increasing from ~18 nm in the early stages of the reaction (1200°C sample) to ~34 nm in the 1400°C sample and ~49 nm in the 1475°C sample. (It was not possible to measure an HfC crystallite size for the 1100°C sample because only a trace of HfC was

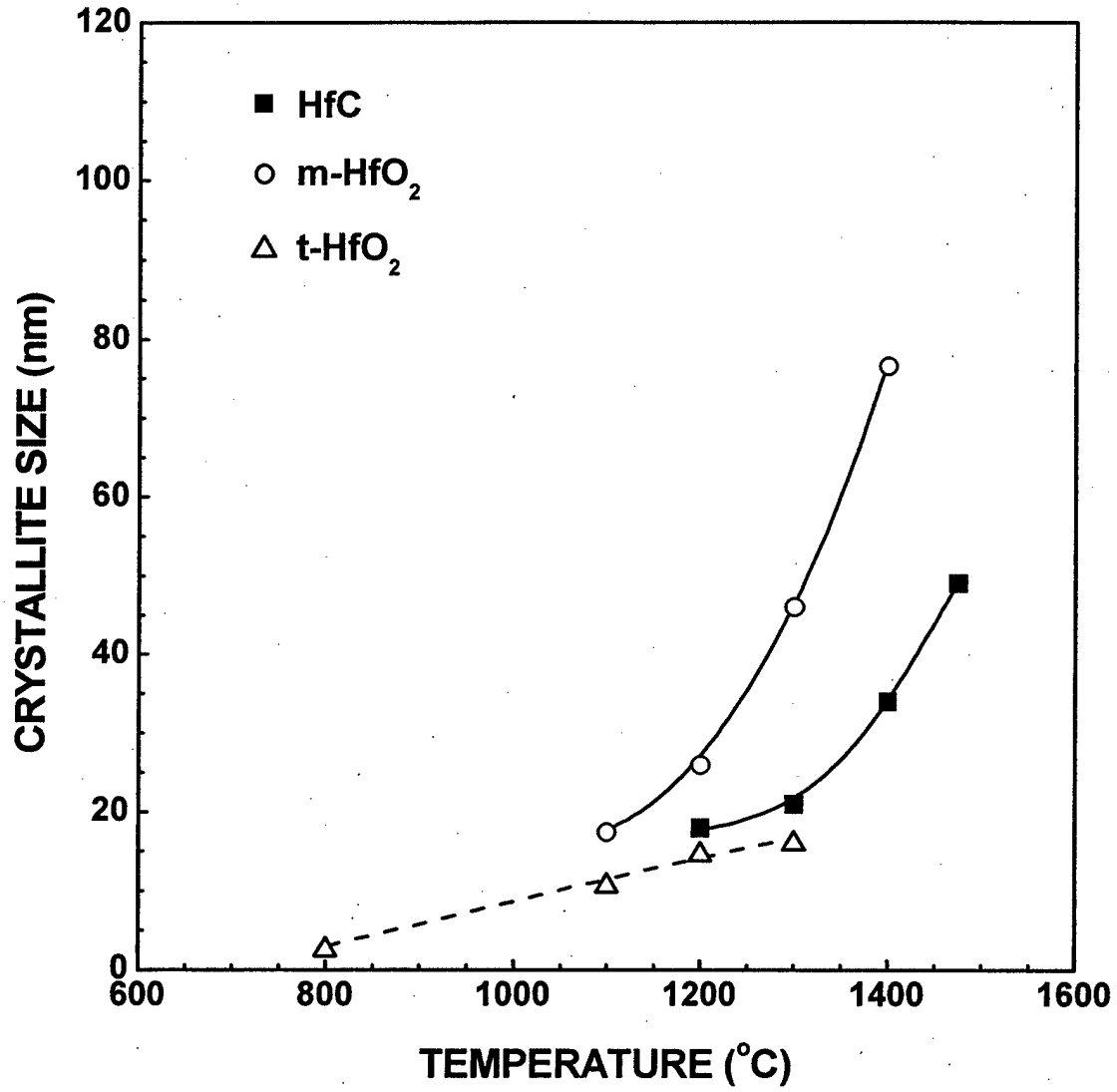

Fig. 13. Plot of the t-HfO_2, m-HfO_2, and HfC crystallite sizes (determined from XRD measurements) vs. heat treatment temperature

surmised to be present based on a slight shoulder at $2\theta \approx 33.4$ degrees.) The HfC crystallite size increased to an estimated size of ~200 nm in the sample heat treated at 1800°C.

The HfC lattice parameter measured for the 1800°C sample was 0.4638 nm which indicates that the composition was near-stoichiometric. (The measured lattice parameter matches the value listed in reference 46. It is also close to values reported for near-stoichiometric HfC by other investigators, although it should be noted that a fairly wide range of values have been reported.[2]) The carbon content measured for the 1800°C sample (6.7 wt%) remained slightly above the value (6.3 wt%) for stoichiometric HfC. However, it was noted earlier that the starting composition (determined for an 1100°C-pyrolyzed sample) was slightly carbon-rich compared to the ideal composition for the reaction analogous to the one shown in eq. (1) for ZrC. Hence, it is reasonable that a small amount of residual carbon would remain in the sample after the carbothermal reduction reaction was completed.

4.3 Silicon Carbide (SiC)

The initial carbothermal reduction experiments were carried out using the 1100°C-pyrolyzed silica/carbon precursor with C/Si molar ratio of 2.4. Figure 14 shows X-ray diffraction (XRD) patterns for the as-pyrolyzed sample and for samples which were heat treated at 1300°C for the indicated times. The as-pyrolyzed sample was XRD-amorphous.

The amount of β-SiC increased as the heat treatment time at 1300°C increased. Weight loss measurements (discussed below) showed that the carbothermal reduction reaction was ~99% completed after the 16 h heat treatment at 1300°C. The low reaction temperature was indicative of the fine scale of mixing of the carbon and silica reactants.

The overall carbothermal reduction reaction is given by:

$$3C_{(s)} + SiO_{2(s)} = SiC_{(s)} + 2CO_{(g)} \qquad (3)$$

There is evidence from previous carbothermal reduction studies that SiC is produced by a multi-step process involving intermediate reactions which generate silicon monoxide (SiO) vapor, transport of the

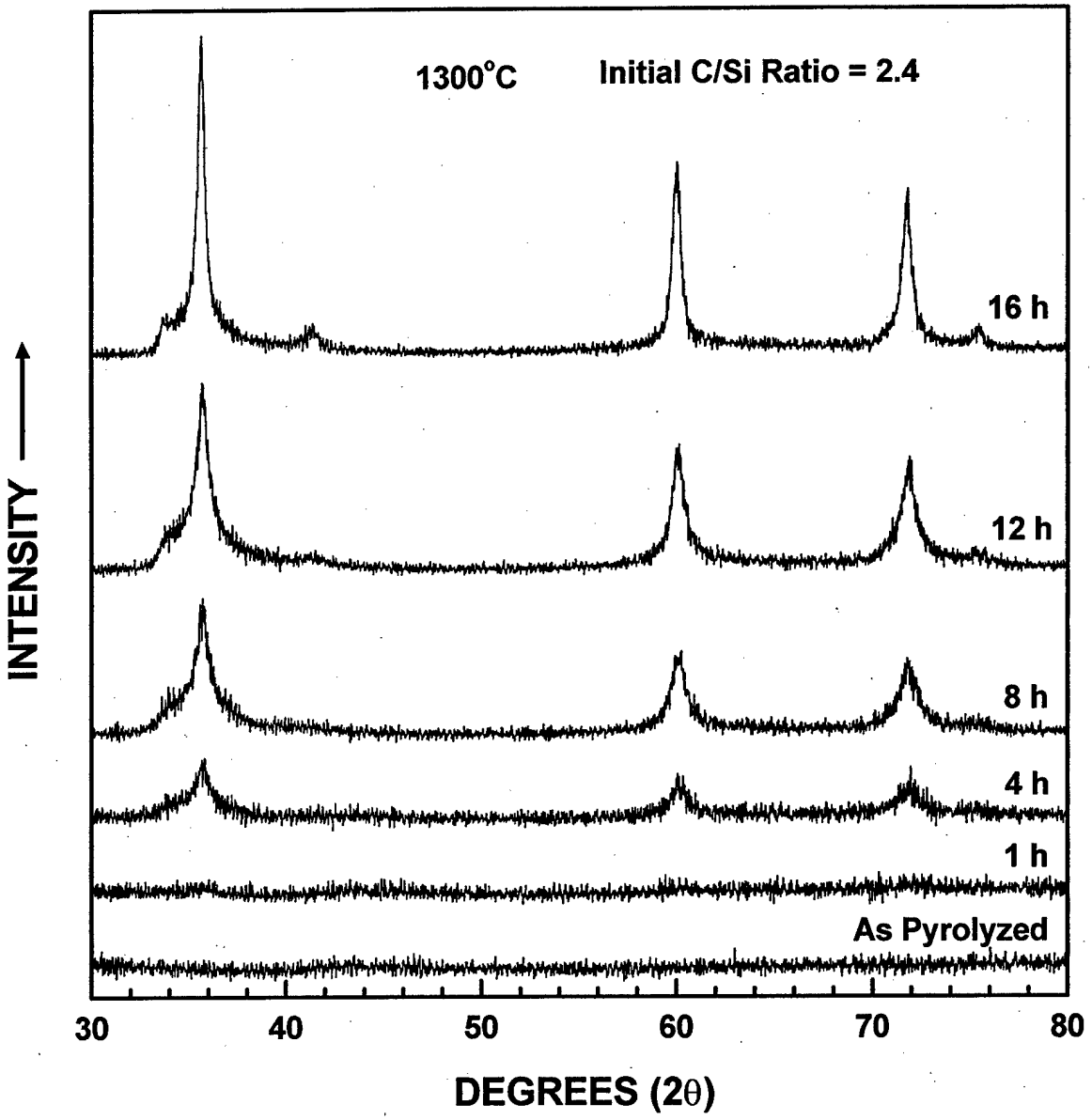

Fig. 14. XRD patterns for an as-pyrolyzed (1100°C) sample with C/Si ratio of 2.4 and for samples subsequently heat treated at 1300°C for the indicated times.

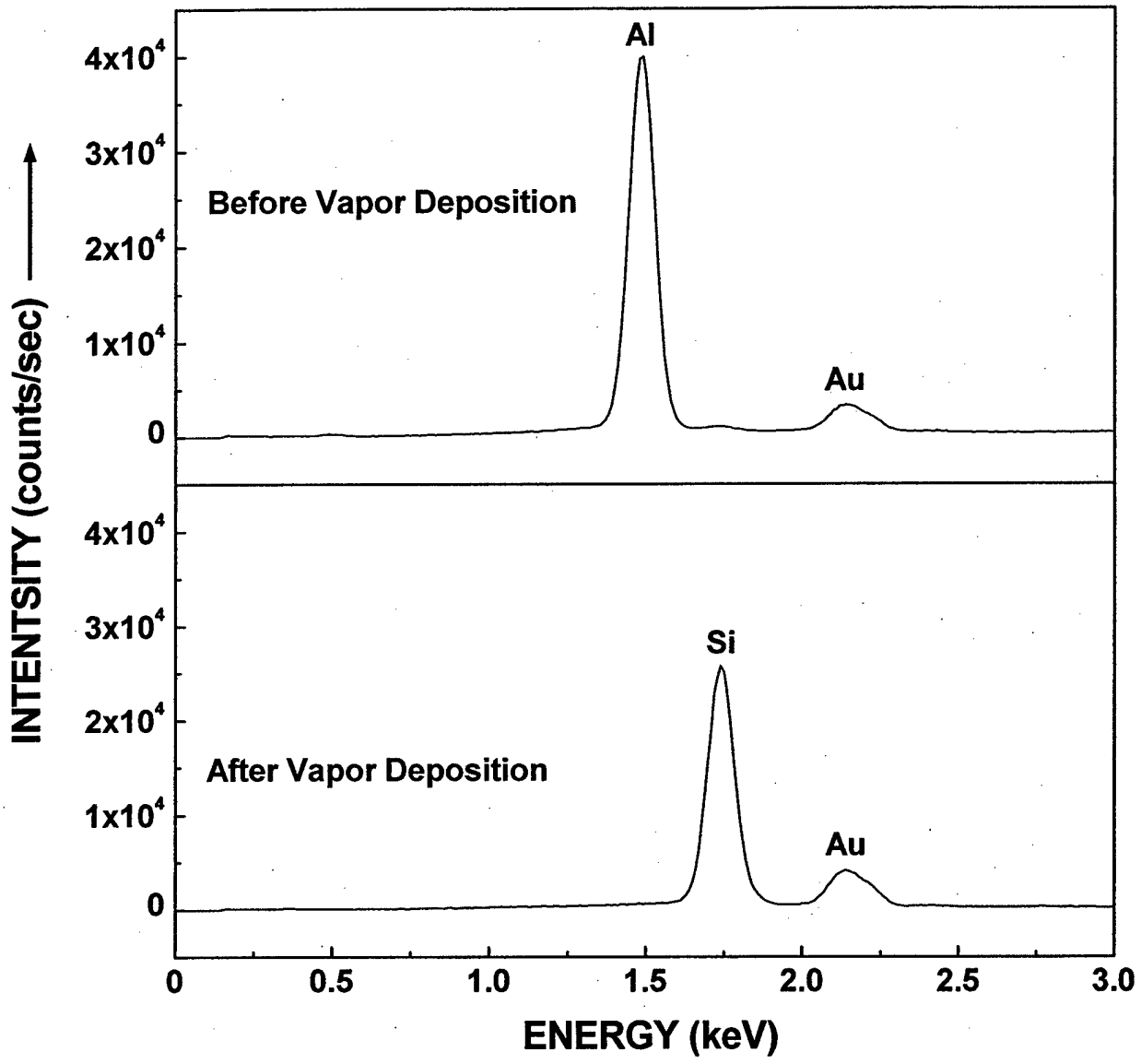

Fig. 15. EDX spectra from the surface of an alumina substrate before and after a vapor deposition experiment carried out at 1160° C for 8 h.

SiO vapor to the carbon phase, and subsequent reaction at the carbon surface to form the SiC.[20-23] Reaction (3) can be broken into the following elementary steps:

$$C_{(s)} + SiO_{2\,(s)} = SiO_{(g)} + CO_{(g)} \quad (4)$$

$$2C_{(s)} + SiO_{(g)} = SiC_{(s)} + CO_{(g)} \quad (5)$$

In the present study, experiments indicated that SiO volatilization occurred from the earliest stage of the reaction. An alumina substrate was placed downstream from an 1100°C-pyrolyzed silica/carbon reaction mixture and the mixture was subsequently heat treated for 8 h at 1160°C. Figure 15 shows the results of EDX elemental analysis of the substrate surface before and after the heat treatment. The Si/Al weight percent ratio was 0.02 for the initial substrate and then increased to 160 for the heat-treated substrate. (The Au peaks in the spectra in Fig. 15 are from sputtered coatings that were deposited so that the substrates would be conductive for SEM observations.)

The extent of the overall reaction given by eq. (3) may be followed by monitoring the sample weight loss, the amount of CO gas evolved, and/or the amount of SiC formed. In this study, the reaction kinetics were determined from measurements of both weight loss and amount of SiC formed. (The SiC content was determined by quantitative X-ray diffraction, QXRD.)

Figure 16 shows plots of fractional weight loss vs. time for samples (with initial C/Si molar ratio of 2.4) that were heat treated at four different temperatures in the range of 1160-1300°C. The fractional weight loss, F, is given by:

$$F = W_{t,T} / W_{max} \quad (6)$$

where $W_{t,T}$ was the observed weight loss for a given time/temperature condition and W_{max} was the maximum weight loss obtained by carbothermal reduction of the 1100°C-pyrolyzed sample. (The latter value was determined by a heat treating sample at 1495°C for 2 h.) As noted earlier, the reaction is nearly completed after heat treatment for 16 h at only 1300°C.

The SiC yield for the ideal carbothermal reduction reaction shown in eq. (3) (in which the C/Si molar ratio is 3) would be 41.7 wt% if the reaction went to completion. (The weight percentage yield is

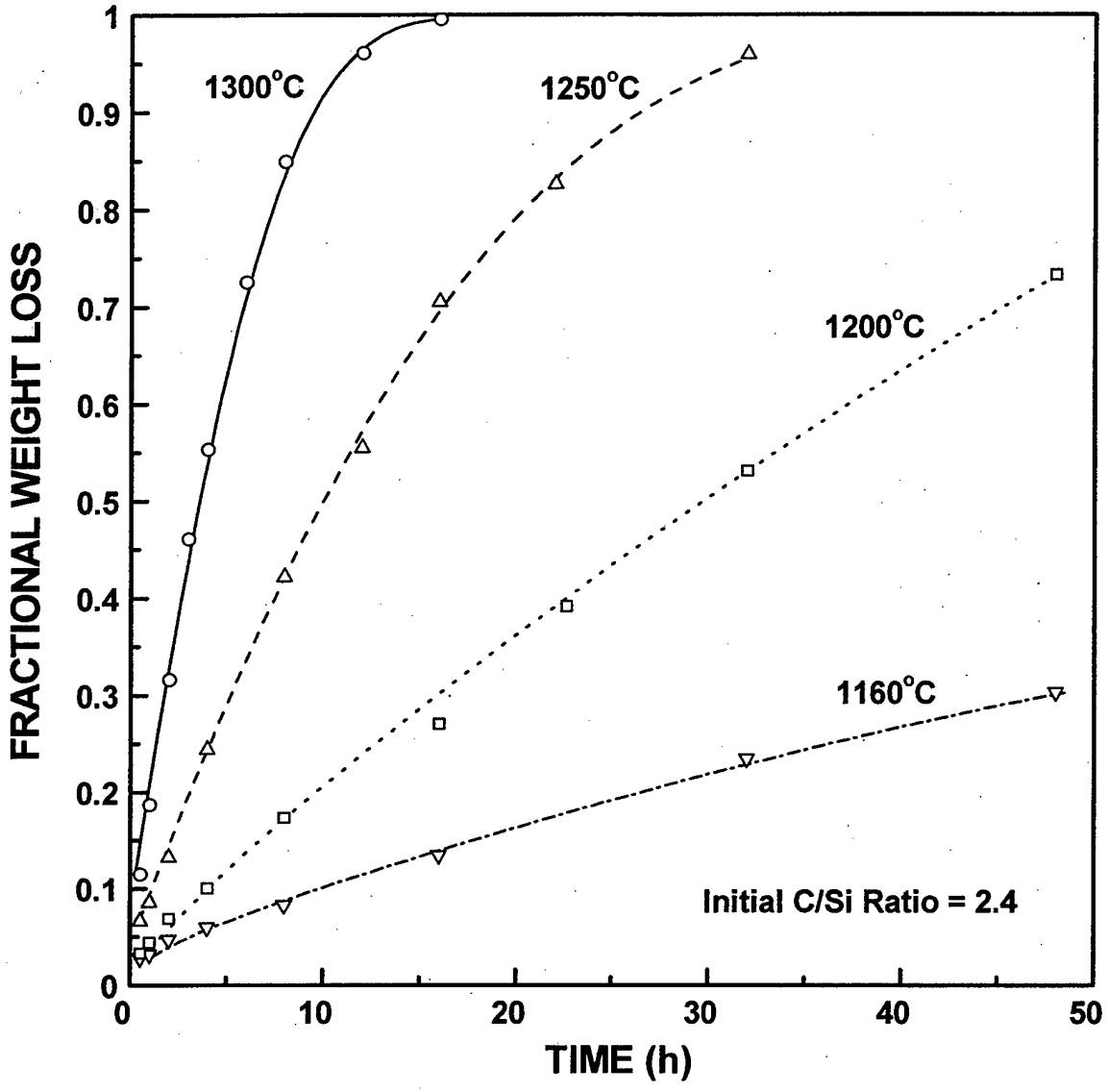

Fig. 16. Plots of fractional weight loss vs. time for samples with initial C/Si ratio of 2.4 which were heat treated at the indicated temperatures.

defined as the weight of SiC product formed divided by the weight of the reactants (3C + SiO_2).) However, the starting composition for the samples in Fig. 16 was silica-rich (i.e., C/Si molar ratio = 2.4) compared to that shown in eq. (3). Hence, a SiC yield of 36.0 wt% would be expected if the following assumptions were made: (i) all the carbon reacted to form SiC according to the reaction stoichiometry indicated in eq. (1) and (ii) all the "excess" SiO_2 in the reactant mixture was eliminated (i.e., via SiO volatilization) without reacting with any of the SiC product that formed as the reaction proceeded. The actual *product* yield observed after complete reaction in this study was only 33 wt%. In addition, carbon analysis indicated that the final product contained ~98 wt% SiC and ~2 wt% "free" (unreacted) carbon, so the SiC yield was ~32.3 wt%. The lower yield indicates that some SiO vapor was swept away from the reaction mixture before participating in the SiC-forming reaction (eq. (5)) and that assumption (ii) was not valid (i.e., some of the "excess" silica was eliminated by reacting with SiC product that formed during the reaction).

Although several previous studies indicate that carbothermal reduction synthesis of SiC occurs via reaction of SiO vapor with carbon, there is no consensus on the specific reaction mechanism. For example, consider the contrasting results obtained in studies by Weimer et al.[22] and Ono and Kurachi.[25] Weimer et al. studied carbothermal reduction using mixtures of fine carbon and silica particles and observed that the reaction kinetics fit the "shrinking core" (or "contracting volume") model. They concluded that rate-controlling step was the reaction to form SiC at carbon surfaces (i.e., eq. (5)). Ono and Kurachi studied carbothermal reduction using sol-gel samples prepared from ethyl silicate/phenolic resin solutions and observed that the reaction kinetics fit the Avrami-Erofe'ev nucleation and growth model. They concluded that the reaction rate was controlled by diffusion of carbon to growing SiC crystallites. In the present study, the weight loss data in Fig. 14 showed the best fit to the reaction-controlled "shrinking core" model, as expressed by the following equation:

$$1 - (1 - X)^{1/3} = kt \qquad (7)$$

where X is the extent of reaction (i.e., fractional conversion to SiC in this case), t is the reaction time,

and k is the rate constant. Figure 17 shows that there is a good fit to equation (7) for almost of the entire range of the reaction.

As noted earlier, quantitative XRD was also used to determine the extent of reaction based on the amount of SiC formed. The results obtained by this method were very similar to those shown in Figs. 16 and 17. Figure 18 shows that the fractional conversion to SiC, determined by QXRD, fits equation (7) well.

The shrinking-core model also appears to be consistent with changes observed in certain structural characteristics (i.e., pore volume and crystallite size) of the reaction product formed by the carbothermal reduction reaction. The 1100°C-pyrolyzed starting material was in the form of relatively coarse particles (<140 mesh) which consisted of a fine-scale amorphous silica/carbon mixture. Gas adsorption measurements showed that these coarse particles had very little internal porosity (i.e., <0.002 g/cm^3). If the "shrinking core" model is applicable to the SiC carbothermal reduction reaction, then the SiC product would initially form at the surface and the reaction interface would progressively "sweep" through to the interior of the coarse particles. However, vapor phase transport is required for the reaction shown in equation (5) to proceed, i.e., SiO vapor must migrate to carbon surfaces and CO vapor must migrate away from the reaction product. Hence, the product must have porosity in order for the reaction to continue to progress from the surface to the interior of the particles. Pore formation was indeed observed in the present study, as shown in Fig. 19. The total specific pore volume (determined by gas adsorption/ condensation) increases from an initial value <0.002 cm^3/g to a maximum value of ~ 0.82 cm^3/g when the fractional weight loss reaches a value of ~ 0.96. The formation of porosity is attributed primarily to the removal of the silica phase from the starting carbon/silica mixture, i.e., via the volatilization reaction shown by eq. (4). The specific pore volume increases as silica is consumed (and as the carbothermal reduction reaction proceeds toward completion). In contrast, the SiC-forming reaction shown in eq. (5) should not have much effect on the amount of porosity formed because the solid reactant (2 moles of C) and solid product (1 mole of SiC) have similar volume. (It is necessary to know the true (solid) density

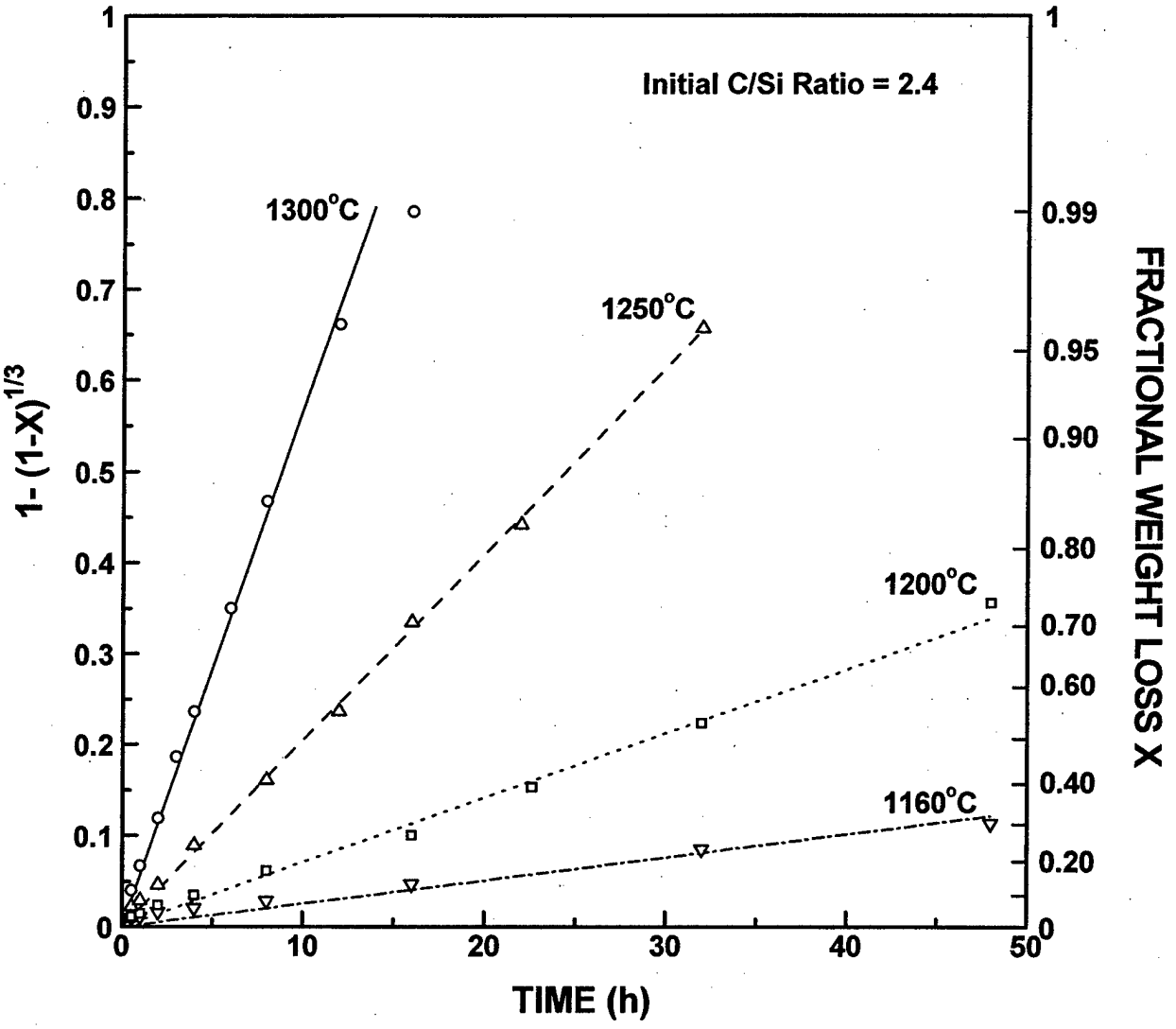

Fig. 17. Plots in which the weight loss kinetic data (for samples prepared with initial C/Si ratio of 2.4) are fit to the reaction equation for the interface-controlled "shrinking core" model

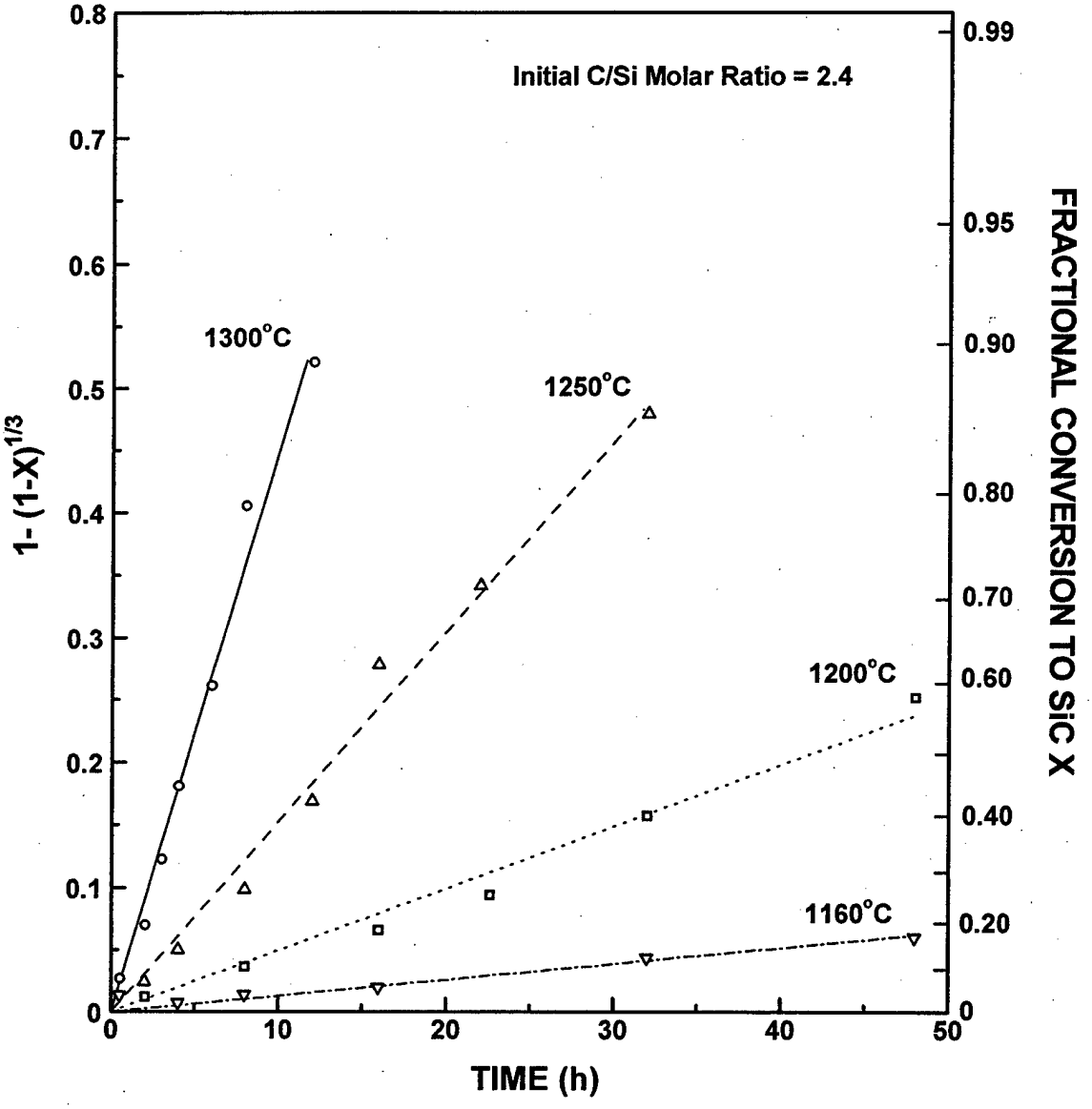

Fig. 18. Plots in which the kinetic data for the fractional conversion to SiC (determined by QXRD for samples with initial C/Si ratio of 2.4) are fit to the reaction equation for the interface-controlled "shrinking core" model.

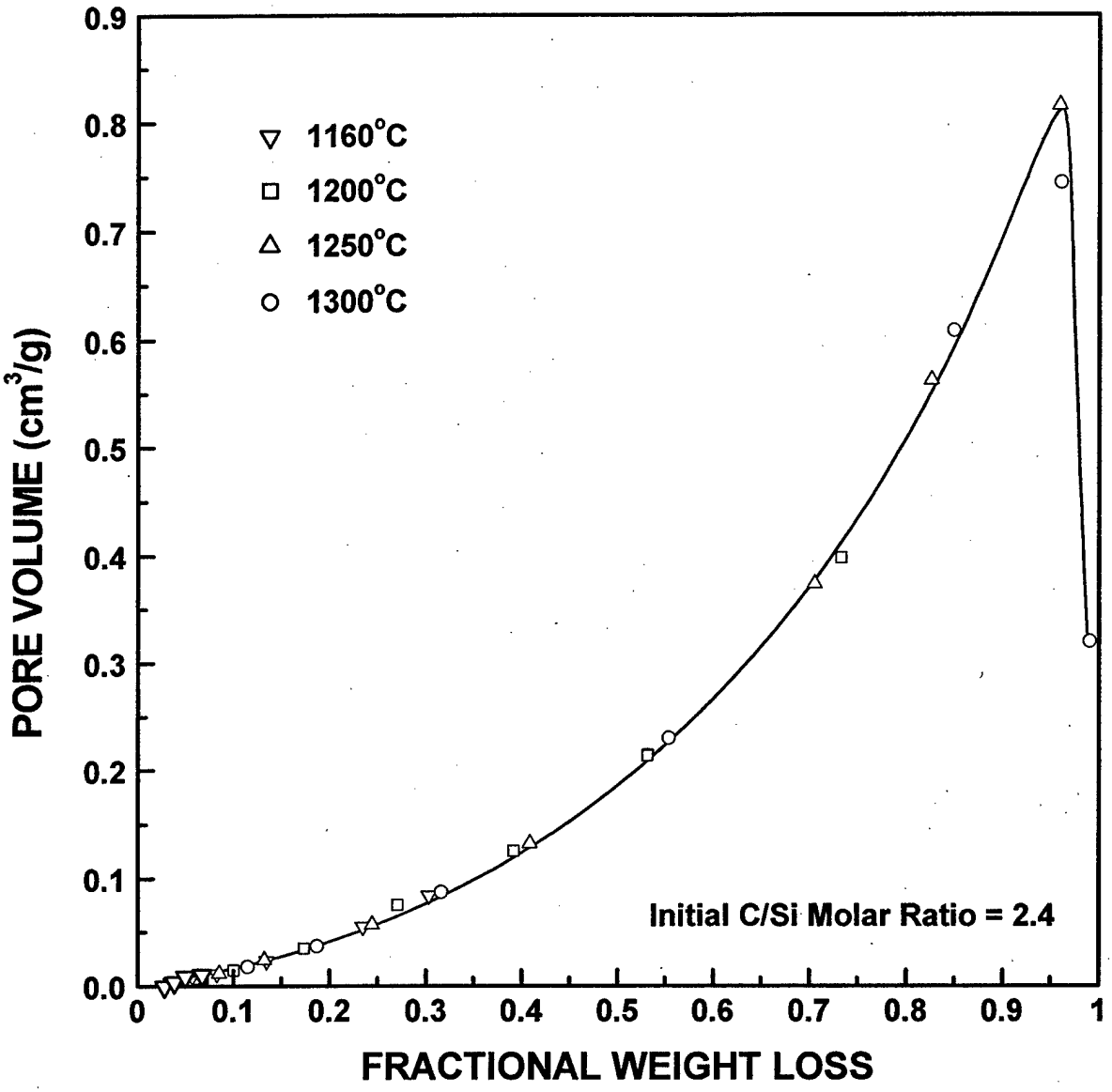

Fig. 19. Plot of specific pore volume vs. the fractional weight loss for heat-treated samples prepared with initial C/Si ratio of 2.4.

values for the carbon and SiC in order to calculate the volume change. These are not known with precision in the present case because the carbon is amorphous and the β-SiC is weakly crystalline. However, reasonable estimates are 1.9-2.1 g/cm^3 and 3.15-3.21 g/cm^3 for amorphous carbon and nanocrystalline β-SiC, respectively.[48,49] These values lead to relatively small volumetric changes, in the range of +11.3% to -1.3%, for the reaction given by eq. (5).)

Figure 19 shows that the porosity decreases sharply during the late stages of the reaction. This observation suggests that some sintering (densification) of the porous SiC product is occurring. Solid-state diffusion in SiC is inhibited when significant amounts of excess ("free") carbon are present. In the late stages of the carbothermal reduction reaction, enough carbon apparently has been removed from localized regions of the sample to permit densification and grain coarsening processes to proceed.

Figure 20 shows the average SiC crystallite size (determined by XRD peak broadening measurements) as a function of the fractional weight loss. Crystallite sizes are not reported for fractional weight loss values below ~0.25 because the XRD peak intensities were too weak to collect reliable data. The average crystallite size showed relatively little change throughout most of the carbothermal reduction reaction. This observation is consistent with the "shrinking core" model in that a uniform product is expected to develop as the reaction "sweeps" through from the surface to the interior regions of the silica/carbon mixture. In the late stages of the reaction, a significant increase in average crystallite size was observed. This increase coincides precisely with the decrease in specific pore volume observed in Fig. 19. As noted earlier, these effects are attributed to enhanced solid-state diffusion resulting from the removal of free carbon from many localized regions of the samples. Despite the grain coarsening that occurs in samples with high degree of conversion (Fig. 20), the average SiC crystallite size still remains less than 25 nm after nearly complete reaction at 1300°C (16 h).

The carbothermal reduction reaction kinetics were also investigated for 1100°C-pyrolyzed samples prepared with a C/Si molar ratio of 4.6 (i.e., a large excess of carbon compared to the C/Si molar ratio of 3 in eq. (3)). Kinetic data were collected over the temperature range of 1160-1250°C. The

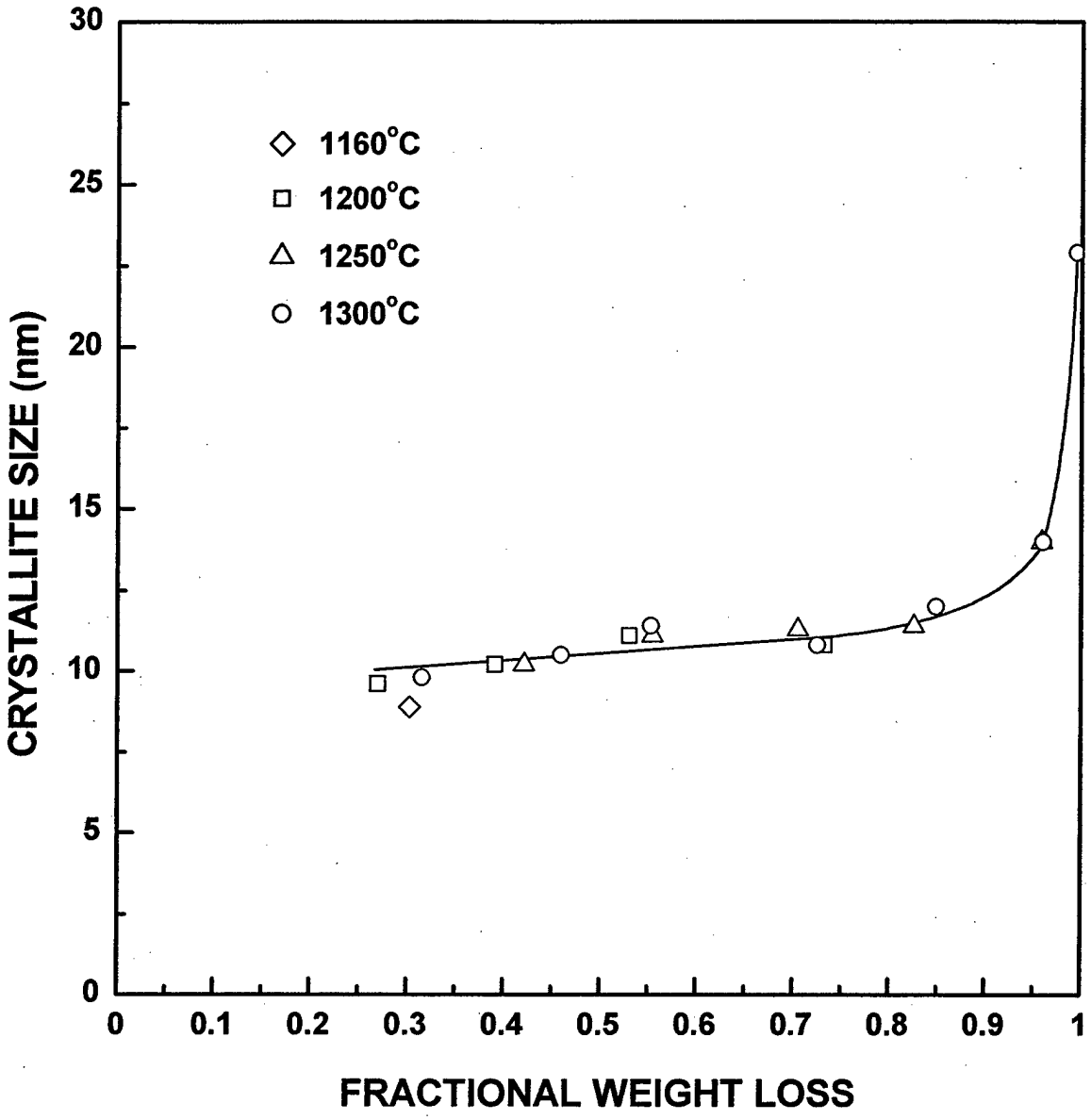

Fig. 20. Plot of SiC average crystallite size vs. the fractional weight loss for heat-treated samples prepared with initial C/Si ratio of 2.4.

results were similar to those in Figs. 16-18 for samples with C/Si molar ratio of 2.4 in that the data showed an excellent fit to the "shrinking core" reaction model (i.e., eq. (7)). Figure 21 shows plots of the logarithm of the rate constants (obtained from weight loss data using eq.(7)) vs. inverse temperature for the samples with the two different compositions. The activation energy values were 414 kJ/mol and 389 kJ/mol for the samples with C/Si molar ratios of 2.4 and 4.6, respectively. (These values are very similar to those reported in the studies by Weimer et al. [22] and Ono and Kurachi.[25]) Since samples for both compositions showed reaction kinetics that fit eq. (7) well and also gave very similar activation energy values, it is likely that the reaction mechanism was independent of the C/Si ratio in the initial mixtures.

Figure 21 also shows that the samples with the higher C/Si ratio had significantly larger rate constants (i.e., approximately three times larger) over the common temperature range of 1160-1250°C. The higher reaction rate is attributed to the larger amount of carbon surface area (per unit sample volume) available for the reaction (i.e., eq. (5)). This explanation is consistent with the proposed "shrinking-core" reaction mechanism in which the rate is controlled by the chemical reaction (eq. (5)) at the carbon surfaces. (A higher reaction rate would be expected with higher carbon specific surface area.)

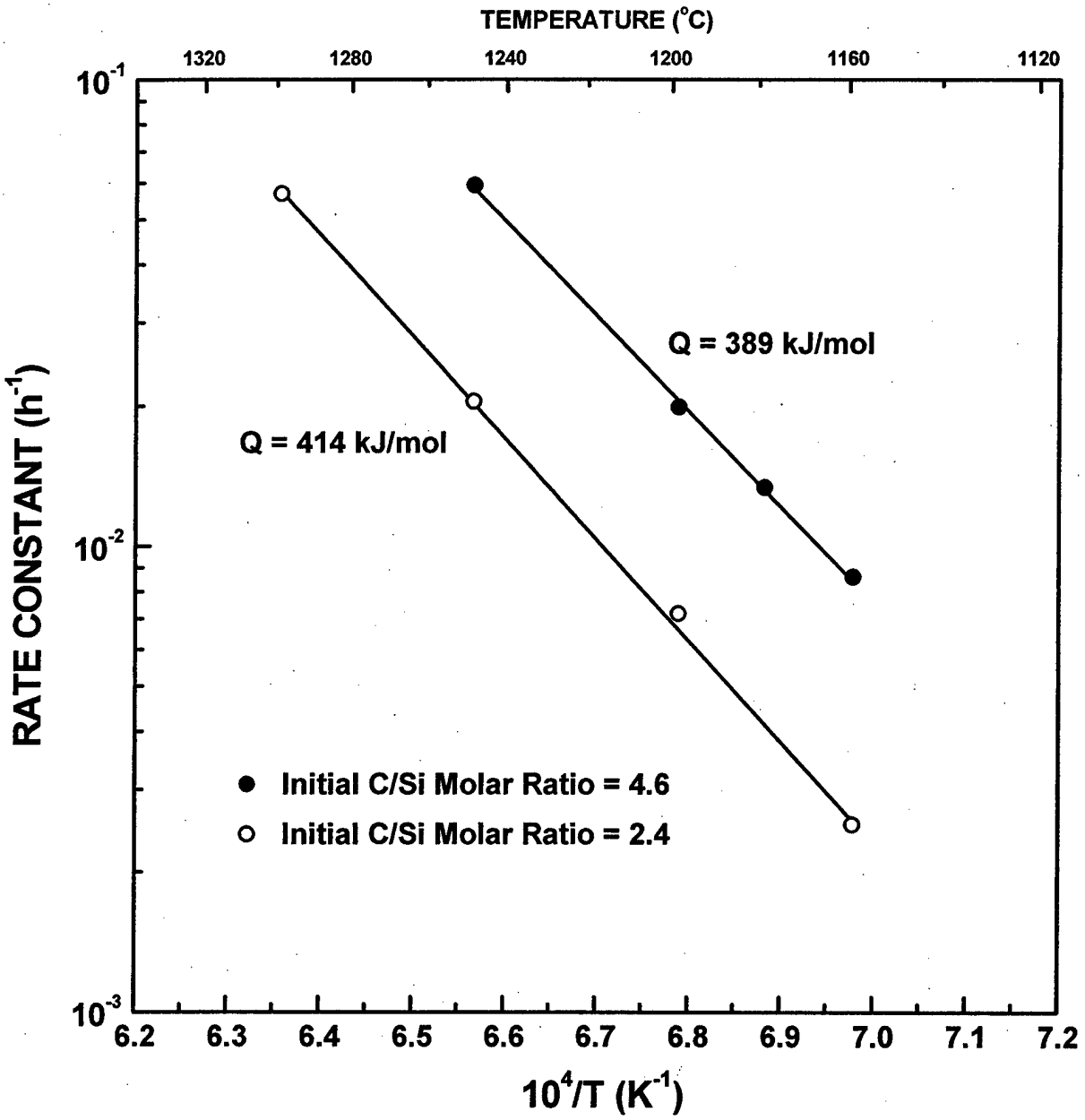

Fig. 21. Plot of reaction rate constant (determined from weight loss data) vs. inverse temperature for samples prepared with initial C/Si ratios of 2.4 and 4.6.

5.0 CONCLUSIONS

5.1 Zirconium Carbide (ZrC) and Hafnium Carbide (HfC)

Zirconium carbide (ZrC) and hafnium carbide (HfC) powders were produced by carbothermal reduction reactions using fine-scale carbon/metal oxide mixtures as the starting materials. The reactant mixtures were prepared by pyrolytic decomposition of solution-derived precursors. The latter precursors were synthesized via hydrolysis/condensation of metal-organic compounds. The first step in the solution process involved refluxing a metal alkoxide with 2,4 pentanedione ("acacH") in order to partially or fully convert the metal alkoxy groups to a chelated metal diketonate structure ("metal acac"). This was followed by the addition of water (under acidic conditions) in order to promote hydrolysis/condensation reactions. Precursors with variable carbon/metal ratios were produced by varying the concentrations of the solution reactants (i.e., the metal alkoxide, "acacH," water, and acid concentrations). In the Hf-based system, "single-source" precursors could be synthesized which yielded powders with C/HfO_2 molar ratios $\approx$ 3.1 after pyrolysis. (This C/HfO_2 ratio was used to produce near-stoichiometric HfC after carbothermal reduction, i.e., according to the Hf-based reaction analogous to eq. (1).) In the Zr-based system, it was necessary to add a secondary soluble carbon source (i.e., phenolic resin or glycerol) during solution processing in order to obtain a C/ZrO_2 molar ratio $\approx$ 3.1 in the pyrolyzed powders.

The phase development during carbothermal reduction was investigated using pyrolyzed powders with carbon/metal oxide molar ratio $\approx$ 3.1. The pyrolyzed powders initially consisted of fine-scale mixtures of the tetragonal phase of the metal oxide (ZrO_2 or HfO_2) and amorphous carbon. The tetragonal phase transformed to the monoclinic phase during heat treatment at or above 1100°C. The initial formation of the metal carbide (ZrC or HfC) was clearly evident after heat treatment at 1200°C and the reaction was substantially completed after heat treatments in the range of ~1400-1500°C. HfC and ZrC crystallite sizes (determined by XRD line broadening) were ~50 nm and ~100-130 nm, respectively, for powders produced at 1475°C. However, weight loss measurements and analyses of the

carbon and oxygen contents showed that these samples consisted of metal carbide with some oxygen dissolved in the lattice and some residual free carbon. Heat treatment at higher temperatures (>1600°C) was required to produce near-stoichiometric metal carbides with low oxygen content.

ZrC powders with ~ 100 nm crystallite size were dry-pressed to form "green" compacts with $\sim 44\%$ relative density. The compacts were sintered at temperatures in the range of 1600-1950°C (2 h). Samples sintered at 1900°C and 1950°C had relative densities of ~ 98 and $\sim 99\%$, respectively, and zero open porosity.

5.2 Silicon Carbide (SiC)

Solution-based processing was used to produce fine-scale carbon/silica mixtures. These mixtures were used for low-temperature carbothermal reduction synthesis of nanocrystalline SiC powders. Reactant mixtures with C/Si molar ratio of 2.4 were transformed almost completely to SiC with average crystallite size <25 nm by heat treatment at 1300°C for 16 h.

The carbothermal reduction reaction mechanism was investigated by (i) analyzing vapor-deposited product formed downstream from the reaction mixture and (ii) measuring the weight loss, amount of SiC formed, specific pore volume, and SiC crystallite size for the reacted samples. The results were consistent with a reaction mechanism in which silicon monoxide (SiO) vapor reacted at the carbon surfaces to form SiC. The reaction kinetics fit a "shrinking core" model in which the interfacial reaction was the rate-controlling step. Higher reaction rates were observed for samples prepared with higher C/Si ratio. This was attributed to the higher specific surface area of carbon in the samples and was consistent with the conclusion that the rate was controlled by the SiC-forming reaction at the carbon surfaces.

6.0 REFERENCES

1. L.E. Toth, Transition Metal Carbides and Nitrides, Academic Press, New York, 1971.

2. A.J. Perry, "The Refractories HfC and HfN - A Survey. I Basic Properties," Powder Metall. Int., 19 [2] 29-35 (1987).

3. K. Upadhya, J.-M. Yan, and W.P. Hoffman, "Materials for Ultrahigh Temperature Structural Applications," Bull. Am. Ceram. Soc., 76 51-56 (1997).

4. R.W. Newman, "Oxidation-Resistant High-Temperature Materials," Johns Hopkins APL Technical Digest, 14 [1] 24-28 (1993).

5. M.M. Opeka, I.G. Talmy, E.J. Wuchina, J.A. Zaykosi, and S.J. Causey, "Mechanical, Thermal, and Oxidation Properties of Refractory Hafnium and Zirconium Compounds," J. Eur. Ceram. Soc., 19 2405-2414 (1999).

6. F.M. Charbonnier, W.A. Mackie, R.L. Hartman, and Tianbao Xie, "Robust High Current Field Emitter Tips and Arrays for Vacuum Microelectronic Devices," J. Vac. Sci. Technol. B, Vol. 19, 1064-1072 (2001).

7. B.V. Cockeram, D.P. Measures, and A.J. Meuller, "The Development and Testing of Emissivity Enhancement Coatings for Thermophotovoltaic (TPV) Radiator Applications," Thin Solid Films, 355-356 17-25 (1999).

8. K. Minato, T. Ogawa, K. Sawa, A. Ishikawa, T. Tomita, S. Iida, and H. Sekino, "Irradiation Experiment on ZrC-Coated Fuel Particles for High-Temperature Gas-Cooled Reactors," Nucl. Technol., 130 272-281 (1999).

9. V.I. Zhelankin, V.S. Kutsev, and B.F. Ormont, "Equilibrium in Reactions for Reduction of ZrO_2 and V_2O_3 by Carbon at High Temperatures," Zh. Neorg. Khim., 3 [5] 1237-1240 (1958).

10. S.K. Sarkar, A.D. Miller, and J.I. Mueller, "Solubility of Oxygen in ZrC," J. Am. Ceram. Soc., 55 [1] 628-630 (1972).

11. C.E. Curtis, L.M. Doney, and J.R. Johnson, "Some Properties of Hafnium Oxide, Hafnium Silicate, Calcium Hafnate, and Hafnium Carbide," J. Am. Ceram. Soc., 37 [10] 458-465 (1954).

12. P.G. Cotter and J.A. Kohn, "Industrial Diamond Substitutes: I, Physical and X-ray Study of Hafnium Carbide," J. Am. Ceram. Soc., 37 [9] 415-420 (1954).

13. R.V. Sara, "The Hafnium-Carbon System," Trans. AIME, 223 1683-1691 (1965)

14. E.L. Sham, E.M. Farfan-Torres, S. Bruque-Gamez, and J.J. Rodriguez-Jimenez, "Synthesis of ZrC/ZrO_2 by Pyrolysis of Modified Zirconium Alkoxide Precursors," Solid State Ionics, 63-65 45-

51 (1993).

15. H. Preiss, E. Schierhorn, K.W. and Brzezinka, "Synthesis of Polymeric Titanium and Zirconium Precursors and Preparation of Carbide Fibers and Films," J. Mater. Sci., 33 4697-4706 (1998).

16. I. Hasegawa, Y. Fukuda, and M. Kajiwara, "Inorganic-Organic Hybrid Route to Synthesis of ZrC and Si-Zr-C Fibres," Ceram. International, 25 523-527 (1999).

17. Z. Hu, M.D. Sacks, G.A. Staab, C.-A. Wang, and A. Jain, "Solution-Based Processing of Nanocrystalline ZrC," Ceram. Eng. Sci. Proc., 23 [4] 711-717 (2002).

18. Y. Kurokawa, S. Kobayashi, M. Suzuki, M. Shimazaki, and M. Takahashi, "Preparation of Refractory Carbide Fibers by Thermal Decomposition of Transition Metal (Ti, Zr, Hf, Nb, Ta) Alkoxide-Cellulose Precursor Gel Fibers," J. Mater. Res., 13 [3] 760-765 (1998).

19. J.S. Reed, Principles of Ceramics Processing, Second Edition, Wiley-Interscience, New York, 1995.

20. J.L. Blumenthal, M.J. Santy, and E.A. Burns, "Kinetic Studies of High-Temperature Carbon-Silica Reactions in Charred Silica-Reinforced Phenolic Resins," AIAA J., 4 [6] 1053-1057 (1966).

21. V.M. Kevorkijan, M. Komac, and D. Kolar, "Low-Temperature Synthesis of Sinterable SiC Powders by Carbothermic Reduction of Colloidal SiO_2," J. Mater. Sci., 27 [10] 2705-2712 (1992).

22. A.W. Weimer, K.J. Nilson, G.A. Cochran, and R.P. Roach, "Kinetics of Carbothermal Reduction Synthesis of Beta Silicon Carbide," AICHE J., 39 [3] 493-503 (1993).

23. J.-G. Lee and I.B. Cutler, "Formation of Silicon Carbide from Rice Hulls," Bull. Am. Ceram. Soc., 54 [2] 195-198 (1975).

24. H. Tanaka and Y. Kurachi, "Synthesis of β-SiC Powder from Organic Precursor and its Sinterability," Ceram. Int., 14 109-115 (1988).

25. K. Ono and Y. Kurachi, "Kinetic Studies of β-SiC Formation from Homogeneous Precursors," J. Mater. Sci., 26 388-392 (1991).

26. G.C. Wei, C.R. Kennedy, and L.A. Harris, "Synthesis of Sinterable SiC Powders by Carbothermic Reduction of Gel-Derived Precursors and Pyrolysis of Polycarbosilane," Bull. Am. Ceram. Soc., 63 [8] 1054-1061 (1984).

27. Y. Sugahara, Y. Takeda, K. Kuroda, and C. Kato, "Carbothermal Reduction Process of Precursors Derived from Alkoxides for Synthesis of Boron-Doped SiC Powder," J. Mater. Sci. Lett., 8 944-946 (1989).

28. B.D. Cullity, in "Elements of X-ray Diffraction" (Addison-Wesley Publishing Co., Reading, MA, 1967).

29. D.C. Bradley, R.C. Mehrohtra, and W. Wardlaw, "Hafnium Alkoxides," J. Chem. Soc. (London), 1634-1636 (1953).

30. C.D. Gagliardi and K.A. Berglund, "Hafnium Metal-Organic Films and Gels Produced by Sol-Gel Processing," pp. 127-135 in Processing Science of Advanced Ceramics, edited by I.A. Aksay, G.L. McVay, D.R. Ulrich, Mat. Res. Soc. Symp. Proc., Vol. 155, Mater. Res. Soc., Pittsburgh, PA, 1989.

31. C.J. Brinker and G.W. Scherer, Sol-Gel Science, Academic Press, San Diego, CA, 1990.

32. K. Constant, R. Kieffer, and P. Ettmayer, "About the Pseudoternary System "ZrO" - ZrN -XrC," Monatshefte fur Chemie, 106 823-832 (1975).

33. A. Ouensanga, A. Pialoux, and M. Dode, "High Temperature X-ray Study of the Zr-O-C System in Thermodynamical Equilibrium Conditions in the Vacuum," Rev. Int. Hautes Temp. Refract., 11 289-294 (1974).

34. A. Maitre and P. Lefort, "Solid State Reaction of Zirconia with Carbon," Solid State Ionics, 104 109-122 (1997).

35. V.P. Bulychev, R.A. Andrievskii, and L.B. Nezhevenko, "The Sintering of Zirconium Carbide," Poroshkovaya Metallurgia, 172 (4), 38-42, 1977.

36. L.B. Nezhevenko, I.I. Spivak, P.V. Gerasimov, B.D. Gurevich, and V.N. Rystsov, "Sintering of Zirconium and Niobium Carbides with Carbon Additions," Poroshkovaya Metallurgia, 212 (8), 23-28, 1980.

37. A.G. Lanin, E.V. Marchev, and S.A. Pritchin, "Non-isothermal Sintering Parameters and their Influence on the Structure and Properties of Zirconium Carbide," Ceramics International, 17 310-307 (1991).

38. P. Barnier, C. Brodhag, and F. Thevenot, "Hot Pressing Kinetics of Zirconium Carbide," J. Mater. Sci., 21 2547-2552 (1986).

39. C.T. Lynch, K.S. Mazdiyasni, J.S. Smith, and W.J. Crawford, "Infrared Spectra of Transition Metal Alkoxides," Anal. Chem., 36(12) 2332-2337 (1964).

40. R.C. Fay and T.J. Pinnavaia, "Infrared and Raman Spectra of Some Six-, Seven-, and Eight-Coordinated Acetylacetonato Complexes of Zirconium (IV) and Hafnium (IV), Inorg. Chem., 7(3) 508-514 (1968).

41. B. Allard, "Studies of Tetravalent Acetylacetonato Complexes - I, Coordination and Properties in the Solid State, "J. Inorg. Nucl. Chem., 38 2109-2115 (1976).

42. Powder Diffraction File Card No. 08-0342 (tetragonal hafnium oxide, HfO_2), JCPDS - International Centre for Diffraction Data, Newtown Square, PA.

43. Powder Diffraction File Card No. 21-0904 (orthorhombic hafnium oxide, HfO_2), JCPDS - International Centre for Diffraction Data, Newtown Square, PA.

44. G. Bocquillon, C. Susse, and B. Vodar, "Allotropie de L'Oxyde d'Hafnium sous Haute Pression," Rev. Int. Hautes Temp. Refract., 5 247-251 (1968).

45. O. Ohtaka, T. Yamanak, and S. Kume, "Synthesis and X-ray Structural Analysis by the Rietveld Method of Orthorhombic Hafnia," J. Ceram. Soc. Jpn, 99 826-827 (1991).

46. Powder Diffraction File Card No. 39-1491 (cubic hafnium carbide, HfC), JCPDS - International Centre for Diffraction Data, Newtown Square, PA.

47. K. Constant, R. Kieffer, and P. Ettmayer, "About the Pseudoternary System "HfO" - HfN - HfC" Monatshefte fur Chemie, 106 973-981 (1975).

48. C.L. Mantell, Carbon and Graphite Handbook, Interscience Publishers, New York, 1968.

49. M.D. Sacks, "Effect of Composition and Heat Treatment Conditions on the Tensile Strength and Creep Resistance of SiC-Based Fibers," J. Eur. Ceram. Soc., 19 2305-2315 (1999).

7.0 APPENDIX

Graduate Student Theses

Anubhav Jain, "Synthesis and Processing of Nanocrystalline Zirconium Carbide Formed by Carbothermal Reduction," M.S. Thesis, Georgia Institute of Technology, August 2004.

Zhe Cheng, "Reaction Kinetics and Structural Evolution for the Formation of Nanocrystalline SiC via Carbothermal Reduction," M.S. Thesis, Georgia Institute of Technology, December 2004.

Refereed Publications

C.-A. Wang, M.D. Sacks, G.A. Staab, and Z. Cheng, "Solution-Based Processing of Nanocrystalline SiC," Ceram. Eng. Sci. Proc., 23(4) 701-709 (2002).

Z. Hu, M.D. Sacks, G.A. Staab, C.-A. Wang, and A. Jain, "Solution-Based Processing of Nanocrystalline ZrC," Ceram. Eng. Sci. Proc., 23(4) 711-717 (2002).

C.-A. Wang and M.D. Sacks, "Processing of Nanocrystalline Hafnium Carbide Powders," Ceram. Eng. Sci. Proc., 24 (4) 33-40 (2003).

A. Jain, M.D. Sacks, C.-A. Wang, M. Middlemas, and Z. Cheng, "Processing of Nanocrystalline Zirconium Carbide Powders," Ceram. Eng. Sci. Proc., 24 (4) 41-49 (2003).

Z. Cheng, C.-A. Wang, and M.D. Sacks, "Synthesis of Nanocrystalline Silicon Carbide Powders," Ceram. Eng. Sci. Proc., 24 (4) 23-32 (2003).

Z. Cheng, M.D. Sacks, C.-A. Wang, and Z. Yang, "Preparation of Nanocrystalline Silicon Carbide Powders by Carbothermal Reduction," pp. 15-25 in *Innovative Processing and Synthesis of Ceramics, Glasses, and Composites VII*, edited by J.P. Singh and N.P. Bansal, Ceramic Transactions, Vol. 154, American Ceramic Society, Westerville, OH, 2003.

C.-A. Wang, M.D. Sacks, and Z. Yang, "Preparation of Nanocrystalline Hafnium Carbide Powders by Carbothermal Reduction," pp. 27-36 in *Innovative Processing and Synthesis of Ceramics, Glasses, and Composites VII*, edited by J.P. Singh and N.P. Bansal, Ceramic Transactions, Vol. 154, American Ceramic Society, Westerville, OH, 2003.

A. Jain, M.D. Sacks, and C.-A. Wang, "Preparation of Nanocrystalline Zirconium Carbide Powders by Carbothermal Reduction," pp. 37-46 in *Innovative Processing and Synthesis of Ceramics, Glasses, and Composites VII*, edited by J.P. Singh and N.P. Bansal, Ceramic Transactions, Vol. 154, American Ceramic Society, Westerville, OH, 2003.

M.D. Sacks, C.-A. Wang, Z. Yang, and A. Jain, "Carbothermal Reduction Synthesis of Nanocrystalline Zirconium Carbide and Hafnium Carbide Powders Using Solution-Derived Precursors," J. Mater. Sci., 392 6057-6066 (2004).